Contents lists available at ScienceDirect

Journal of Alloys and Compounds

journal homepage: www.elsevier.com

Giant magnetoimpedance in rapidly quenched materials

A. Zhukov [a, b, c, *], M. Ipatov [a, b], P. Corte-León [a, b], L. Gonzalez- Legarreta [a, d], M. Churyukanova [e], J.M. Blanco [b], J. Gonzalez [a], S. Taskaev [f], B. Hernando [g], V. Zhukova [a, b]

[a] Basque Country Univesity, UPV/EHU, San Sebastián, 20018, Spain
[b] EIG, Basque Country Univesity, UPV/EHU San Sebastián, 20018, Spain
[c] IKERBASQUE, Basque Foundation for Science, Bilbao, 48011, Spain
[d] Inorganic Chemistry-University of Cantabria, Nanomedice-IDIVAL, Avda. de Los Castros 46, 39005, Santander, Spain
[e] National University of Science and Technology «MISIS», Moscow, 119049, Russia
[f] NRU South Ural State University, Chelyabinsk, 454080, Russia
[g] Oviedo University, Spain

ARTICLE INFO

Article history:
Received 12 April 2019
Received in revised form 31 July 2019
Accepted 9 September 2019
Available online xxx

Keywords:
Soft magnetic materials
Giant magnetoimpedance
Magnetoelastic anisotropy
Magnetostriction
Nanocrystals

ABSTRACT

We present an overview of the factors as well as post processing tools allowing optimization of magnetic softness and GMI effect of rapidly quenched materials: microwires and ribbons. Generally, low coercivity and high GMI effect have been observed in as-prepared Co-rich compositions. Annealing at adequate conditions can be very effective for manipulation of the magnetic properties and GMI effect of amorphous and nanocrystalline rapidly quenched materials. After annealing of Co-rich compositions, we can observe transformation of inclined hysteresis loops to rectangular. However, at certain annealing conditions GMI effect can be improved. Using stress-annealing, GMI effect of both Fe-rich and Co-rich microwires as well as of amorphous ribbons can be improved. On the other hand, in Fe-rich FeCuNbSiB microwires after appropriate annealing we observed considerable magnetic softening and GMI effect enhancement. The other promising post-processing allowing GMI effect optimization is Joule heating.

1. Introduction

Magnetic materials belong to a family of the most promising materials, which are demanded in diverse applications, like generation and distribution of electricity, data storage, medicine, home entertainment, electronic surveillance, automobile and aircraft industries, aerospace, energy harvesting and conversion, informatics, magnetic recording, magnetic sensors and telecommunications among others [1–4].

Magnetic materials are classified in terms of their magnetic properties and their uses. If a material is easily magnetized and demagnetized then it is referred to as a soft magnetic material, whereas if it is difficult to demagnetize then it is referred to as a hard (or permanent) magnetic material [3–5].

Soft magnetic materials typically present coercivity below 1000 A/m. They are used primarily to enhance and/or channel the magnetic flux produced by an electric current, for shielding applications or to generate a magnetic field. However, one of the features of soft magnetic materials quite relevant for magnetic sensors and devices is so-called giant magnetoimpedance (GMI) [5–11]. The origin of the GMI effect as well as the main characteristics of GMI are satisfactorily explained in terms of classical electrodynamics, taking into account the skin effect of a soft magnetic conductor [5–11]. High magnetic permeability of crystalline or amorphous magnetic materials is a prerequisite for the implementation of the GMI effect [5–8,10,11].

Magnetic softness of conventional magnetic materials is linked to their crystalline structure, defects, grain size, texture, etc. Therefore, crystalline magnetic materials require additional post-processing to achieve better magnetic softness [1–3].

Consequently, amorphous magnetic materials obtained using rapid solidification (also frequently called rapid quenching) from the melt have attracted special attention since their discovery in the 60-s [12–14]. One of the main advantages of amorphous magnetic materials is that excellent magnetic softness can be obtained directly in the as-cast samples without additional post-processing. In addition, the fabrication method, including rapid solidification from the melt, is quite fast and inexpensive. Furthermore, amorphous materials as a rule present superior mechanical properties [15–18].

Magnetic softness of rapidly solidified from the melt alloys is associated to their liquid-like structure characterized by the absence of all the defects typical for crystalline materials [3–5].

Therefore, although GMI materials are not restricted to amorphous materials [6], the latter are recognized by most of researchers as the most prospective in terms of the GMI effect [7,8,10,11]. Among the other GMI materials, nanocrystalline and nanostructured materials should be mentioned [19–23]. Indeed, in some cases nanocrystallization of amorphous precursor by appropriate annealing allows beneficial improvement of magnetic softness [14,19] as

* Corresponding author. Basque Country Univesity, UPV/EHU, San Sebastián, 20018, Spain.
Email address: arkadi.joukov@ehu.es (A. Zhukov)

https://doi.org/10.1016/j.jallcom.2019.152225
0925-8388/

well as the GMI effect [20–23]. However, the mechanical properties of nanocrystalline materials are an issue: usually nanocrystallization is associated with an abrupt deterioration of mechanical properties and embrittlement [18].

On the other hand, the use of nanostructured materials, such as thin films and multilayers, allows miniaturization of sensors and devices utilizing the GMI effect [24-28]. In addition, thin-film GMI elements are more compatible with integrated electronic devices. However, as a rule, thin films present much poorer magnetic softness [29] and, hence, the GMI effect, exhibited by nanostructured materials, is several times lower than that of amorphous wires and ribbons [24–27].

Indeed, the main interest and advantages of the GMI effect is that GMI materials can present extremely high sensitivity to applied magnetic field.

The most commonly used expression for the GMI effect is the GMI ratio, $\Delta Z/Z$, usually defined as [10,11]:

$$\Delta Z/Z = [Z(H) - Z(H_{max})] / Z(H_{max}), \quad (1)$$

where H_{max} is the maximum axial *DC* magnetic field (usually up to few kA/m).

The highest GMI ratio is reported for amorphous microwires [30–32]: optimization of preparation conditions allowed achieving $\Delta Z/Z \approx 615\%$ in magnetic microwires [30]. Appropriate post-processing allowed improving $\Delta Z/Z$ up to 600% [31] and 650% [32]. Similarly, $\Delta Z/Z$ ˜640% is achieved upon nanocrystallization of amorphous ribbons [33].

Consequently, the giant impedance sensitivity exerted by magnetically soft amorphous materials stimulated the development and implementation of magnetometers and magnetic field sensors utilizing GMI materials [25,34–39]. GMI technology has been proposed for numerous applications, like magnetic compass and acceleration sensors integrated in CMOS circuit [34,35], low-sized magnetometer suitable for magnetic field mapping [36], detection of a biomagnetic field with the pico-Tesla sensitivity [37] or magnetoelastic sensors [38]. Amorphous wires are used for almost all reported sensors.

Comparative analysis of various sensor technologies (Hall-effect, Magnetoresistance, Fluxgates and GMI effect) allowed to conclude that the GMI- based magnetic sensor technology provides quite competitive features (low dimensions, noise, high magnetic field resolution, etc.) as-compared to analysed technologies [34,39].

Other factors relevant to GMI applications are the miniaturization of soft magnetic materials, tuneability of their magnetic properties and cost efficiency, which allows the development of low-cost modern magnetoelectronic devices with reduced dimensionality and better performance. However, theoretically predicted skin depth minimum is about 0,2–0,3 μm [40,41]. Additionally, thin films technology does not allow achievement of magnetic softness comparable to that reported for rapidly solidified amorphous materials [29]. Indeed, extremely soft magnetic properties with coercivity values of about 2–5A/m and magnetic anisotropy field of about 25 A/m are reported for amorphous Co-rich microwires [32,42]. The problem of compatibility of the MI elements made from amorphous wires with integrated electronic devices is already solved [34,43–45].

As mentioned above magnetic softness is the principle requirement for the GMI ratio optimization. Furthermore, in ferromagnetic materials the domain structure must be considered and consequently the magnetic permeability and hence magnetoimpedance have the tensor nature [8,46]. From the viewpoint of applications the antisymmetrical magnetic field dependence of the off-diagonal GMI component of amorphous wires measured as the output voltage from the pick-up coil surrounding the magnetic wire presenting linear dependence on applied magnetic field is quite useful for applications in magnetic sensors [34,35,44,45].

The main route for the development of the GMI materials is related to development of low dimensional rapidly solidified amorphous materials.

The highest GMI and most of experimental studies deal with different families of magnetic wires. It is commonly accepted that high circumferential magnetic permeability is essentially beneficial for implementation of high GMI ratio [5–8,10,11,42,46].

There are several families of magnetic wires that can be prepared using various methods involving rapid solidification from the melt and hence providing wide range of diameter (from 185 nm reported for glass-coated microwires up to about 165 μm for wires prepared by in-rotating water method) [47–49].

The thinnest magnetic wires with diameters ranging from about 200 nm up to 100 μm can be prepared by so-called modified Taylor-Ulitovsky method (also known as quenching-and-drawing method) [30–32,42,47,48,50]. This technique allows to vary the diameters of the metal nucleus of glass-coated microwires by almost 2 orders of magnitude, covering the most suitable geometry for GMI materials. The Taylor-Ulitovsky preparation method in its present form is known since 60-s [51] and first reports on preparation of magnetic microwires are dated by the end of 70-s [52]. The main advantages of this method are wide range of metallic nucleus diameters, almost continuous preparation method (up to 10000 m long continuous microwire) and presence of thin flexible and biocompatible glass coating allowing better corrosion and mechanical properties [42,53,54].

However, presence of glass-coating is associated with certain peculiarities, like additional magnetoelastic anisotropy related to strong internal stresses induced during rapid solidification of metallic alloys surrounded by glass coating with different thermal expansion coefficients [53–55]. Additionally, a formation of the interfacial layer (with typical thickness of the order of 0,5 μm) between the metallic nucleus and glass-coating is reported for both Fe- and Co-based microwires [56].

In spite of excellent GMI characteristics exhibited by amorphous and nanocrystalline materials with GMI ratios up to 650% [30–33], reported GMI ratio is still below 3000% theoretically predicted for materials with transverse magnetic anisotropy [40,41].

Present paper provides an overview of the routes allowing optimization of the GMI effect in amorphous and nanocrystalline materials prepared by rapid solidification from the melt.

2. Experimental details

Studied Co-rich and Fe-rich glass-coated microwires have been prepared by Taylor-Ulitovsky technique (also called in some publications as the drawing and quenching technique) described elsewhere [30–32,51–56].

Amorphous Co-rich ribbons have been fabricated by the melt-spinning technique using a Fe wheel as described in Ref. [57].

The compositions and geometry (diameters, thickness and width) of studied samples are provided in Table 1.

Magnetic field dependencies of impedance, Z, and GMI ratio, $\Delta Z/Z$ (defined by eq. (1)), have been measured using a micro-strip sample holder placed inside a sufficiently long solenoid that creates a homogeneous magnetic field, H, with maximum value, H_{max}, up to 20 kA/m. The set-up used to measure the giant magnetoimpedance is shown in Fig. 1.

Impedance components measurements were carried out on the as-prepared and annealed samples soldered to a specially designed

Table 1
Compositions and geometry of analysed GMI materials.

Composition	Metallic nucleus diameter, *d*, (μm) for microwires or width (mm) for ribbons	Total diameter, *D*, (μm) for microwires or thickness (μm) for ribbons	Ratio *ρ*
$Co_{69.2}Fe_{4.1}B_{11.8}Si_{13.8}C_{1.1}$	25.6	30.2	0.84
$Co_{67}Fe_{3.85}Ni_{1.45}B_{11.5}Si_{14.5}Mo_{1.7}$	16.8	24	0.7
$Co_{67}Fe_{3.85}Ni_{1.45}B_{11.5}Si_{14.5}Mo_{1.7}$	11.8	18.4	0.64
$Co_{67}Fe_{3.85}Ni_{1.45}B_{11.5}Si_{14.5}Mo_{1.7}$	9.8	18.6	0.5
$Co_{67}Fe_{3.85}Ni_{1.45}B_{11.5}Si_{14.5}Mo_{1.7}$	6.8	13.5	0.5
$Fe_{75}B_9Si_{12}C_4$	15.2	17.2	0.88
$Fe_{47.4}Ni_{26.6}Si_{11}B_{13}C_2$	29	32.2	0.9
$Fe_{70.8}Cu_1Nb_{3.1}Si_{14.5}B_{10.6}$	11.2	14.4	0.8
$Co_{77.5}Si_{15}B_{7.5}$	13.1	18	0.73
$Co_{67}Fe_{3.9}Ni_{1.4}B_{11.5}Si_{14.5}Mo_{1.6}$	25.6	26.6	0.96
$Co_{67.7}Fe_{4.3}Ni_{1.6}Si_{11.2}B_{12.4}C_{1.5}Mo_{1.3}$	10.8	13.8	0.78
$Fe_{6.1}Co_{57}Ni_{10}B_{15.9}Si_{11}$	20.4	24	0.85
$Fe_{61}Co_{57}Ni_{10}B_{15.9}Si_{11}$	22.8	25.6	0.89
$Fe_{6.1}Co_{57}Ni_{10}B_{15.9}Si_{11}$	30	32.3	0.93
$Fe_{3.6}Co_{69.2}Ni_1B_{12.5}Si_{11}Mo_{1.5}C_{1.2}$	25.6	30.2	0.85
$Co_{51}Fe_8Ni_{18}B_{13}Si_{10}$	12.8	15.8	0.82
$Co_{66.5}Fe_{3.5}Si_{12.0}B_{18.0}$	0.3–0.9	20	–
$(Co_{0.95}Fe_{0.05})_{75}Si_{10}B_{15}$	0.5	32	–

micro-strip sample holder (see Fig. 1b). In addition, this system allows the application of a transversal bias field H_B created by dc bias current I_b applied to the sample by a bias-tee element. This system is connected to a vector network analyser N5230A (VNA), which allows measuring simultaneously the longitudinal and off-diagonal impedance components of the sample in the frequency range of 10 MHz–3500 MHz [41,57,58]. The longitudinal impedance component is obtained from the reflection coefficient S_{11} by:

$$Z_{zz} = Z_0 \frac{(1 + S_{11})}{(1 - S_{11})} \quad (2)$$

where $Z_0 = 50\,\Omega$ is the characteristic impedance of the electric coaxial line. The off-diagonal impedance component is measured through the transmission coefficient S_{21} as a voltage induced in a 2 mm long pick-up coil wound around the sample (see Fig. 1b). This sample holder allows measuring the samples up to 10 mm length.

The analyser power output in all measurements here presented was 10 mW that corresponds to a 1.4 mA high frequency driving current passing through the sample.

The off-diagonal, $Z_{z\phi}$, component can be found through transmission coefficient, S_{21} [42].

Hysteresis loops of as-prepared and annealed samples were measured by the induction method with a magnetic field applied along the sample axis as described elsewhere [48]. In most of the cases we represent the normalized magnetization, M/M_o, versus magnetic field, H, where M is the magnetic moment at given magnetic field and M_o - is the magnetic moment of the sample at the maximum magnetic field amplitude, H_o.

For the GMI measurements the sample length was 6 mm. For the hysteresis loops evaluation the sample length was 7 cm. In fact the sample length, l, strongly affects the wires domain structure and hence both GMI effect and hysteresis loops [8,24,48]. However, for glass-coated microwires with diameters about 15 μm the influence of the sample length become irrelevant $l \geq 1$ mm [48].

The samples have been annealed with and without stress in conventional furnace at temperatures, T_{ann}, of 200–600 °C for duration, t_{ann}, from 5 to 120 min. In the case of ribbon samples, the vacuum chamber was used. Insulating and continuous glass-coating allows annealing of glass-coated microwires on air.

The stress during the annealing of glass-coated microwires within the metallic nucleus and glass shell has been evaluated as described earlier [59].

Structure and phase composition have been checked using a BRUKER (D8 Advance) X-ray diffractometer with Cu K_α ($\lambda = 1.54$ Å) radiation.

The magnetostriction coefficient of studied samples has been measured using small angle magnetization rotation (SAMR) method described elsewhere [60]. Initially this method has been developed for magnetic materials where the magnetization rotation plays the determining role [60]. Recently, this method has been extended for the successfully employed of magnetic microwires in which only the outer domain shell present magnetization rotation process [61].

3. Experimental results and discussion

3.1. Magnetic microwires

3.1.1. Tuning of GMI effect in as-prepared microwires

As mentioned above, theoretically and experimentally shown elsewhere [46,59] the GMI ratio value and the magnetic field dependence of GMI effect of magnetic materials are determined by easy magnetic anisotropy direction and magnetic anisotropy field as well as by magnetic softness of the material.

As discussed elsewhere [42] for amorphous materials characterized by the absence of magneto-crystalline anisotropy the main sources of magnetic anisotropy are the shape and

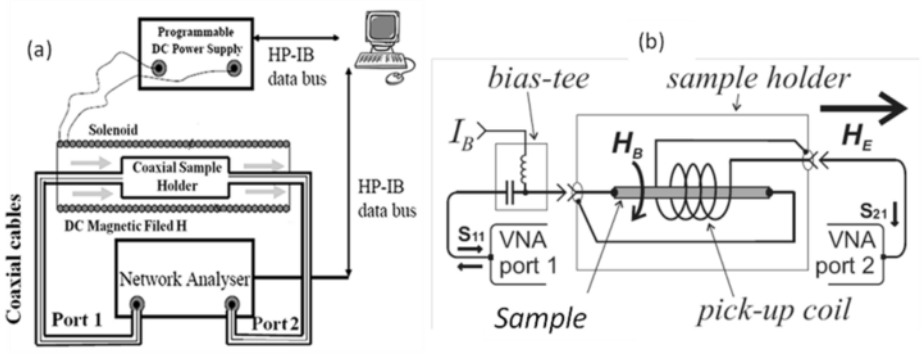

Fig. 1. Experimental set-up for measuring the GMI response of studied samples.

magnetoelastic anisotropy, K_{me}. The latter is determined by the magnetostriction coefficient, λ_s, and the internal stresses, σ_i, by the relation [42]:

$$K_{me} = 3/2\ \lambda_s \sigma_i, \quad (3)$$

The magnetostriction coefficient, λ_s, value in amorphous alloys can be tailored by the chemical composition [14,61–63]. Generally, Fe-rich compositions present positive λ_s -values (typically $\lambda_s \approx 20–40 \times 10^{-6}$), while for the Co-rich alloys, λ_s –values are negative, typically $\lambda_s \approx -5$ to - 3×10^{-6}. Consequently, nearly-zero λ_s –values can be achieved in the Co_xFe_{1-x} ($0 \le x \le 1$) or Co_xMn_{1-x} ($0 \le x \le 1$) systems at x about 0,9–0,96 [14,38,61–63].

In Ni_xFe_{1-x} system decrease of λ_s -values with increasing of Ni-content is observed, but it correlates to the simultaneous decreasing of the saturation magnetization. Thus, zero λ_s –values at high Ni-contents correspond to paramagnetic ordering of Ni_xFe_{1-x} alloys at room temperature [14].

Certainly, such notable dependence of the magnetostriction coefficient, λ_s, on chemical composition of the alloy considerably affects the magnetic properties in particular overall magnetic anisotropy of glass-coated microwires. The reason is quite elevated internal stresses inside the metallic ferromagnetic nucleus of glass-coated microwires distributed in a complex way. The origin of the internal stresses is associated to three main phenomena: i) rapid solidification from the melt of the metallic alloy ingot; ii) the difference between the thermal expansion coefficients of solidifying metallic alloy and glass coating and iii) the drawing of composite wire [53–55,66,67]. The internal stresses distribution is affected by various parameters, as diameter of metallic nucleus, glass-coated thickness and chemical composition of the alloy among others. From the evaluated radial distribution of the internal stresses within the metallic nucleus [66] can be assumed that the axial internal stresses are the strongest within the main part of the metallic nucleus. Thus, the internal stresses distribution along the microwire radius is not homogeneous: near the axis of the metallic nucleus, the tensile stresses are the strongest ones. Such internal stresses distribution together with the sign and value of the magnetostriction coefficient give rise to macroscopic magnetic anisotropy distribution within the ferromagnetic nucleus and hence can strongly affect the GMI ratio value and magnetic field dependence.

Indeed, as can be appreciated from Fig. 2, there is certain correlation between the maximum $\Delta Z/Z$-value, $\Delta Z/Z_{max}$, $\Delta Z/Z\ (H)$ dependencies and the magnetostriction coefficient value and sign. The λ_s –values provided in Fig. 2 are obtained using SAMR method described above.

Both Co-rich microwires present double-peak $\Delta Z/Z(H)$ dependencies (see Fig. 2 (c) and (d)). In fact such double-peak $\Delta Z/Z(H)$ dependencies are theoretically predicted [46] and experimentally reported [42] for magnetic wires with circumferential magnetic anisotropy. The highest $\Delta Z/Z_{max}$ ratio is observed for Co-rich microwire with vanishing λ_s –values. In contrast, the decay observed in the $\Delta Z/Z(H)$ dependencies for both microwires with positive λ_s –values (Fig. 2 (a) and (b)) are predicted and previously observed for magnetic wires with axial magnetic anisotropy [42,46]. $Fe_{75}B_9Si_{12}C_4$ microwire with highest λ_s –value presents the lowest $\Delta Z/Z_{max}$-value (see Fig. 2 (a)).

The observed $\Delta Z/Z(H)$ dependencies correlate well with hysteresis loops. Different magnetic anisotropy of Fe and Co-rich microwires can be appreciated from Fig. 3 where the hysteresis loops of the same samples as in Fig. 2 are provided. Perfectly rectangular hysteresis loops observed for both microwires with positive λ_s –values reflect the axial magnetic anisotropy of these samples (Fig. 3 (a) and (b)). $Fe_{75}B_9Si_{12}C_4$ microwire exhibits a higher coercivity, H_c, which must be related to higher λ_s –values.

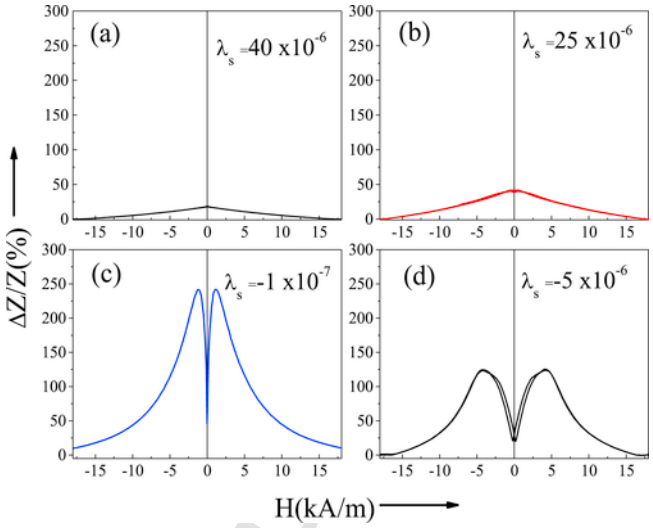

Fig. 2. ΔZ/Z (H) dependencies of as-prepared $Fe_{75}B_9Si_{12}C_4$ (a) $Fe_{47.4}Ni_{26.6}Si_{11}B_{13}C_2$ (b), $Co_{67.1}Fe_{3.8}Ni_{1.4}Si_{14.5}B_{11.5}Mo_{1.7}$ (c) and $Co_{77.5}Si_{15}B_{7.5}$ (d) microwires measured at 500 MHz.

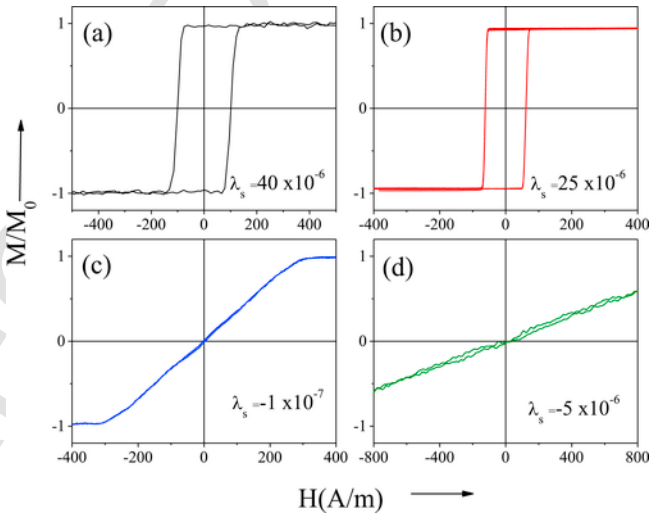

Fig. 3. Hysteresis loops of as-prepared $Fe_{75}B_9Si_{12}C_4$ (a) $Fe_{47.4}Ni_{26.6}Si_{11}B_{13}C_2$ (b), $Co_{67.1}Fe_{3.8}Ni_{1.4}Si_{14.5}B_{11.5}Mo_{1.7}$ (c) and $Co_{77.5}Si_{15}B_{7.5}$ (d) microwires.

$Co_{67.1}Fe_{3.8}Ni_{1.4}Si_{14.5}B_{11.5}Mo_{1.7}$ and $Co_{77.5}Si_{15}B_{7.5}$ microwire with vanishing (≈-1 $x10^{-7}$) and negative (≈-5 $x10^{-6}$) λ_s –values present quite low H_c-values (about 5 A/m), however, much lower magnetic anisotropy field, H_k, (about 300 A/m) is observed for $Co_{67.1}Fe_{3.8}Ni_{1.4}Si_{14.5}B_{11.5}Mo_{1.7}$ microwire (see Fig. 3 (c) and (d)). Furthermore, both Co-rich microwires exhibit linear hysteresis loops typical for microwires with transverse magnetic anisotropy.

The internal stresses value, σ_i, can be tuned by the ρ-ratio between the metallic nucleus diameter, d, and the total microwire diameter, D ($\rho = d/D$): σ_i increases with the increase of the glass coating thickness, i.e., decreasing the ρ-ratio [54,55,65–67]. Therefore, ρ-ratio in fact is the other parameter that can affect both hysteresis loops and hence $\Delta Z/Z_{max}$-value and $\Delta Z/Z(H)$ dependencies of magnetic microwires.

Hysteresis loops of two Co-rich microwires ($Co_{67}Fe_{3.85}Ni_{1.45}B_{11.5}Si_{14.5}Mo_{1.7}$ and $Fe_{6.1}Co_{57}Ni_{10}B_{15.9}Si_{11}$) with vanishing λ_s –values are presented in Fig. 4. In both cases the same tendency is observed, that is, an increase in H_k –values with a decrease in the ρ-ratio (see Fig. 4 (a) and (b)) as also recently

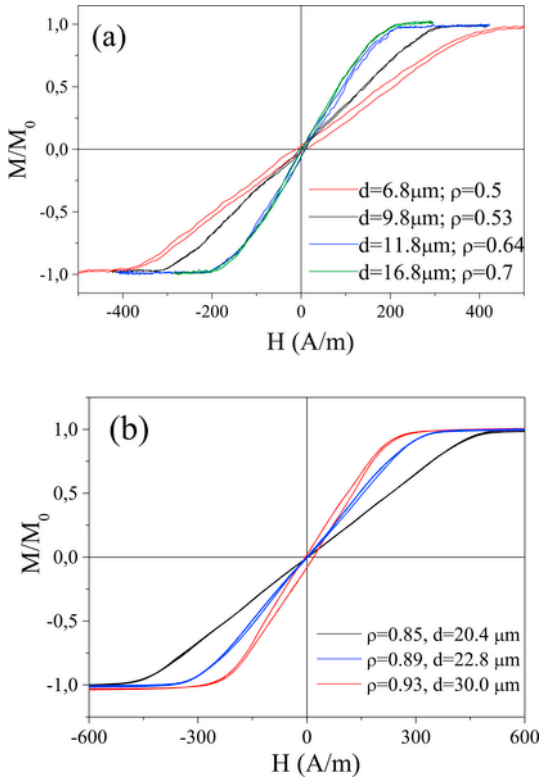

Fig. 4. Hysteresis loops of as-prepared $Co_{67}Fe_{3.85}Ni_{1.45}B_{11.5}Si_{14.5}Mo_{1.7}$ (a) and $Fe_{6.1}Co_{57}Ni_{10}B_{15.9}Si_{11}$ (b) microwires with different diameters.

reported in Ref. [42]. Consequently, *ΔZ/Z(H)* dependencies are affected by *ρ*-ratio (see Fig. 5). Similar dependencies have been previously reported for various Co-rich microwires elsewhere [30,42,64].

Among the other factors relevant for the GMI ratio optimization at a given frequency the diameter of ferromagnetic metallic nucleus must be mentioned.

As an example, *ΔZ/Z(H)* dependencies measured in two as-prepared microwires with quite similar chemical compositions ($Co_{67}Fe_{3.9}Ni_{1.4}B_{11.5}Si_{14.5}Mo_{1.6}$ and $Co_{67.7}Fe_{4.3}Ni_{1.6}Si_{11.2}B_{12.4}C_{1.5}Mo_{1.3}$) but with different dimensions (d=25.6 μm, D=26.6 μm and d=10.8 μm, D=13.8 μm, respectively) are shown in Fig. 6 (a) and (b). The first impression from Fig. 6 (a) (in which the measurements taken at 100 MHz are shown) is that thicker microwires present better GMI performance. However, at 700 MHz the opposite tendency is observed (see Fig. 6 (b)). Observed dependencies are summarized in Fig. 6 (c), where $\Delta Z/Z_{max}(f)$ dependence for both samples are presented for comparison.

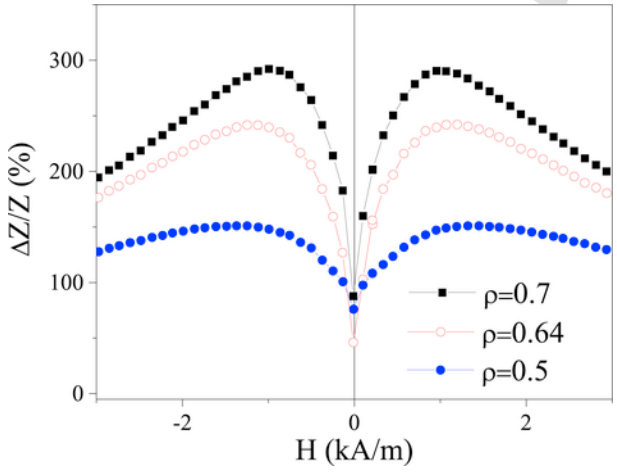

Fig. 5. *ΔZ/Z(H)* dependencies of as-prepared $Co_{67}Fe_{3.85}Ni_{1.45}B_{11.5}Si_{14.5}Mo_{1.7}$ microwires with different *ρ*–ratios measured at 500 MHz.

The observed behaviour confirms the relationship between the optimal frequency for the GMI performance and the wire diameter: to achieve the maximum GMI effect a trade-off between wire dimensions and frequency is required [68]. The diameter reduction must be associated with the increasing of the optimal GMI frequency range [68]. It must be mentioned that this approach is valid with some limitations. The reason is the interfacial layer between the glass coating and metallic nucleus reported for glass-coated microwires [52]. Since the chemical composition of the interfacial layer is different from the inner part of the metallic nucleus, different magnetic anisotropy and therefore different GMI properties can be expected in the surface layer.

One more effective method allowing tuning of the $\Delta Z/Z_{max}$-value and *ΔZ/Z(H)* dependencies of magnetic microwires is the bias current [41,59,69]. The influence of the bias current has been explained considering the circumferential magnetic field, H_{circ}, produced by the current (Oersted field) that can be estimated in the surface of the metallic nucleus from the

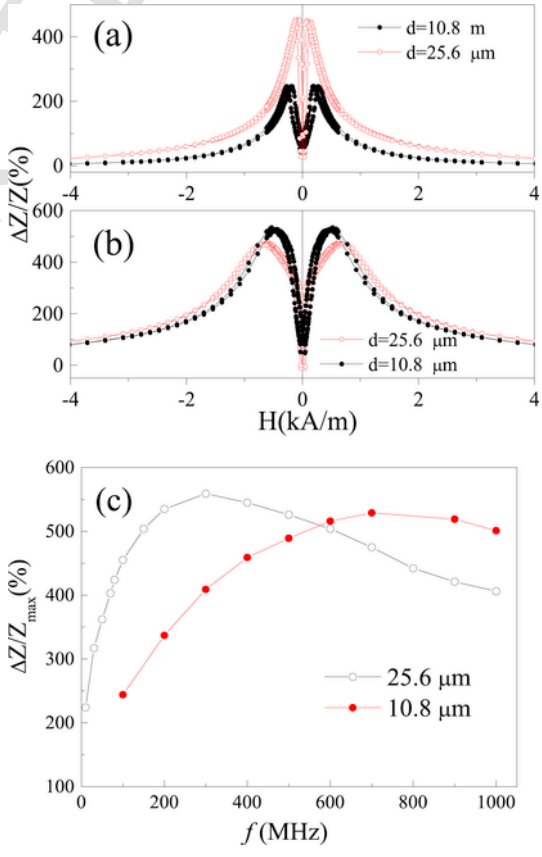

Fig. 6. *ΔZ/Z*(H) dependencies measured in as-prepared $Co_{67}Fe_{3.9}Ni_{1.4}B_{11.5}Si_{14.5}Mo_{1.6}$ (d=25.6 μm, D=26.6 μm) and $Co_{67.7}Fe_{4.3}Ni_{1.6}Si_{11.2}B_{12.4}C_{1.5}Mo_{1.3}$ (d=10.8 μm, D=13.8 μm) microwires at 100 MHz (a), 700 MHz (b) and $\Delta Z/Z_{max}(f)$ dependence for both microwires.

formula:

$$H_{circ}=I_b/2\pi r \quad (4)$$

where I_b is the bias current value, r-radial distance.

The influence of the bias current on GMI ratio of Co-rich and Fe-rich microwires is shown in Fig. 7. Slight increase of the GMI ratio upon effect of the bias current is observed in $Co_{69.2}Fe_{4.1}B_{11.8}Si_{13.8}C_{1.1}$ microwires (Fig. 7 (a)). However, this sample exhibits considerable hysteresis in $\Delta Z/Z(H)$ dependences. This hysteresis is similar to that caused by the core-shell interaction and helical anisotropy [59,70].

More significant effect of bias current on $\Delta Z/Z_{max}$-value and $\Delta Z/Z(H)$ dependencies is observed for as-prepared $Fe_{75}B_9Si_{12}C_4$ microwires (see Fig. 7 (b)), as also recently reported in Ref. [69]. Without bias current as-prepared $Fe_{75}B_9Si_{12}C_4$ microwires exhibit $\Delta Z/Z_{max}\approx 15\%$ at 500 MHz. Upon application of bias current we observed considerable increasing of $\Delta Z/Z_{max}$ up to 60% and even change of the $\Delta Z/Z(H)$ dependencies (Fig. 7 (b)).

H_{circ} –values obtained from eq. (4) for the $Fe_{75}B_9Si_{12}C_4$ microwire ($d=15.2\,\mu m$) for $I_b=50$ mA give $H_{circ}\approx 1$ kA/m. This field is high enough to tilt the magnetization near the surface from the radial direction (it has been assumed for magnetic wires with positive magnetostriction coefficient). Therefore, under application of axial magnetic field the sample can present higher circumferential permeability and therefore higher $\Delta Z/Z_{max}$ and double peak $\Delta Z/Z(H)$ dependencies.

Off-diagonal MI effect, S_{21}, measured in both as-prepared samples present considerable differences (Fig. 8): $Co_{69.2}Fe_{4.1}B_{11.8}Si_{13.8}C_{1.1}$ microwires present rather higher S_{21}-values (Fig. 8 (a)). Additionally, S_{21}-values of $Co_{69.2}Fe_{4.1}B_{11.8}Si_{13.8}C_{1.1}$ microwires rapidly

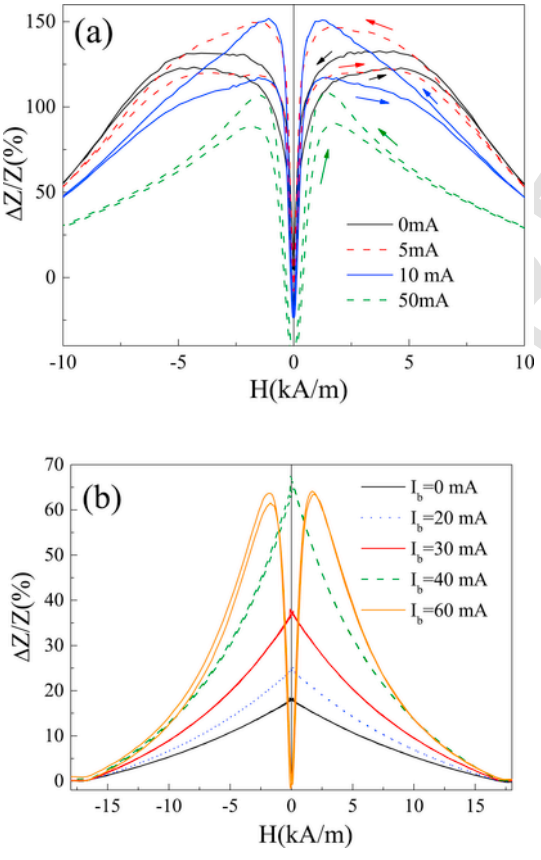

Fig. 7. $\Delta Z/Z(H)$ dependences measured in as-prepared (a) $Co_{69.2}Fe_{4.1}B_{11.8}Si_{13.8}C_{1.1}$ and (b) $Fe_{75}B_9Si_{12}C_4$ microwires measured at 500 MHz at different Ib-values.

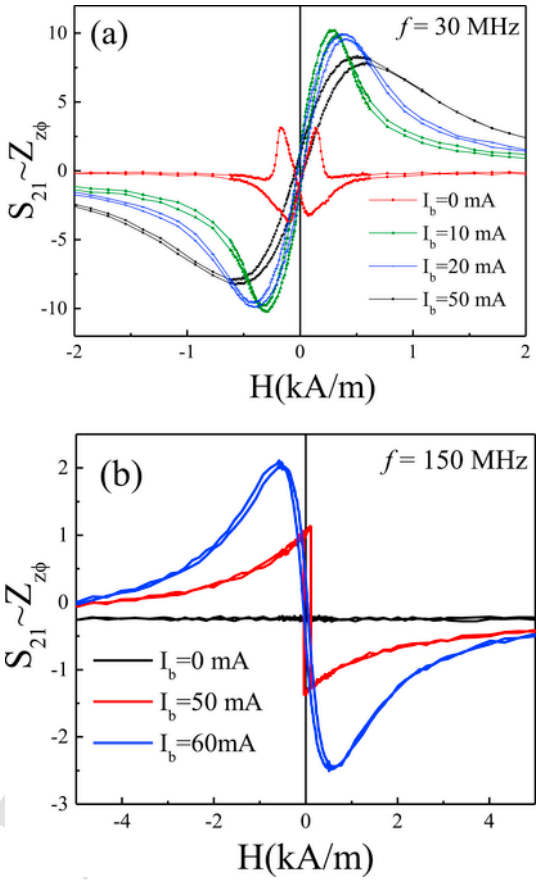

Fig. 8. $S_{21}(H)$ dependences measured in as-prepared (a) $Co_{69.2}Fe_{4.1}B_{11.8}Si_{13.8}C_{1.1}$ and (b) $Fe_{75}B_9Si_{12}C_4$ microwires.

increase upon application of bias current, I_b. $Fe_{75}B_9Si_{12}C_4$ microwire exhibit quite low S_{21}-values (Fig. 8 (b)). We observe increasing of S_{21}-values upon application of the bias current in $Fe_{75}B_9Si_{12}C_4$ sample, but even at $I_b=60$ mA S_{21}-values are a few times lower than those in $Co_{69.2}Fe_{4.1}B_{11.8}Si_{13.8}C_{1.1}$ microwires at $I_b=0$ mA.

Consequently, bias current allows beneficial enhancement of both GMI ratio and off-diagonal MI especially for Fe-rich microwires.

However, these values of DC current flowing through the sample can produce Joule heating of the samples. Indeed, for $Fe_{75}B_9Si_{12}C_4$ microwire ($d\approx 15.2\,\mu m$), the current density, j, for $I_b=60$ mA is about 330 A/mm^2. As shown earlier, the DC current with density $j\tilde{}450$A/mm^2 can produce the magnetic hardening and/or crystallization of the samples [71]. Therefore, application of high enough bias current can produce irreversible structural changes due to annealing.

3.1.2. Tuning of GMI effect of microwires by post-processing

Although generally quite high maximum GMI ratio values (up to 600%) have been realized in as-prepared microwires [30,64], these values are still much below 3000% theoretically predicted $\Delta Z/Z_{max}$ –values for materials with transverse magnetic anisotropy [40,41].

On the other hand, Co belongs to critical raw materials [72]. Consequently, the insecure supplies of Co could hinder the development of new technologies related to massive applications. Additionally, the cost of Co is more elevated. Therefore, Fe-based microwires are preferable for large-scale applications. However, as shown above, as-prepared Fe-rich microwires present generally much poorer GMI performance than Co-rich microwires [42].

Therefore, there are generally two main lines in development of magnetic microwires with GMI effect: i) optimization of GMI effect and magnetic softness in Co-rich microwires by appropriate post-processing and ii) search for adequate post-processing to optimize the effect of GMI in Fe-rich microwires.

The most convenient post-processing allowing stress relaxation is thermal treatment. In amorphous materials, the coercivity decrease is expected upon annealing at temperature below the crystallization temperature due to the stress relaxation [14].

However, in most of recently studied Co-rich microwires with vanishing λ_s –values ($Co_{69\cdot2}Fe_{4\cdot1}B_{11\cdot8}Si_{13\cdot8}C_{1.1}$, $Co_{68\cdot7}Fe_4Ni_1B_{13}Si_{11}Mo_{2.3}$, $Fe_{3\cdot85}Co_{67\cdot05}Ni_{1\cdot44}B_{11\cdot53}Si_{14\cdot47}Mo_{1.66}$, etc.) a considerable magnetic hardening (coercivity and remanent magnetization rising) is reported [73,74].

Below we present results on effect of annealing on magnetic properties of $Fe_{3\cdot6}Co_{69\cdot2}Ni_1B_{12\cdot5}Si_{11}Mo_{1\cdot5}C_{1.2}$ (d=25.6 μm, D=30.2 μm), $Co_{51}Fe_8Ni_{18}B_{13}Si_{10}$ (d=12.8 μm, D=15.8 μm), $Co_{69\cdot2}Fe_{4\cdot1}B_{11\cdot8}Si_{13\cdot8}C_{1.1}$ (d=25.6 μm, D=30.2 μm) and $Co_{67}Fe_{3\cdot9}Ni_{1\cdot5}B_{11\cdot5}Si_{14\cdot5}Mo_{1.6}$ (d=25.6 μm, D=d=26.6 μm) amorphous microwires.

All as-prepared microwires present linear hysteresis loops with low coercivity, H_c (below 10 A/m in both cases). Such hysteresis loops are typical for Co-rich microwires with vanishing λ_s –values (see Fig. 4). However, similarly to those reported for other Co-rich microwires [73,74], we observed considerable magnetic hardening upon annealing: coercivity rising by about an order of magnitude and considerable growth of remanent magnetization (see Fig. 9).

Observed evolution of magnetic properties is related to transformation of linear hysteresis loop with low coercivity ($H_c \approx 4$ A/m) into rectangular with $H_c \approx 90$ A/m upon annealing without stress (see Fig. 9). It is worth noting that $Fe_{3\cdot6}Co_{69\cdot2}Ni_1B_{12\cdot5}Si_{11}Mo_{1\cdot5}C_{1.2}$ samples annealed at different temperatures present similar coercivity, however, the remanent magnetization, M_r/M_{max}, gradually grows upon T_{ann} increasing (see Fig. 9 (b)).

Previously deterioration of the GMI ratio related to magnetic hardening is reported after conventional furnace annealing [73]. However, previously reported results were obtained at fixed annealing conditions.

Below we will present more detailed studies on effect of annealing on GMI effect of $Fe_{3\cdot6}Co_{69\cdot2}Ni_1B_{12\cdot5}Si_{11}Mo_{1\cdot5}C_{1.2}$ microwires. Experimental results provided below and more complex dependence: following the initial decrease of GMI effect after annealing at T_{ann}=200 °C an increase of the GMI ratio is observed at further T_{ann} rising (see Fig. 10 (a) and (b)). Furthermore, the *ΔZ/Z(H)* dependence of as-prepared and annealed sample present rather different features: for as-prepared sample double-peak *ΔZ/Z(H)* dependence (see Fig. 10) is observed. However, *ΔZ/Z(H)* dependence of the sample annealed at 300 °C measured at 50 MHz presents a decay with magnetic field increase (Fig. 10 (a)). The *ΔZ/Z(H)* dependence of the sample annealed at 200 °C still presents double-peak *ΔZ/Z(H)* dependence. But the field value, corresponding to the maximum on *ΔZ/Z(H)* dependence, H_m, is lower than that for as-prepared sample.

On the other hand, even the sample annealed at 300 °C presents double-peak *ΔZ/Z(H)* dependence at f=200 MHz (Fig. 10 (b)). This influence can be understood considering frequency dependence of the skin penetration depth, δ, as well as magnetic anisotropy distribution within the metallic nucleus.

Indeed, frequency dependence of the penetration skin depth, δ, is given by Refs. [7–11]:

$$\delta = \left(\pi\sigma \cdot \mu_\varphi \cdot f\right)^{1/2} \quad (5)$$

where σ is the electrical conductivity and μ_φ - the circumferential magnetic permeability.

At relatively low frequency, the skin depth can be comparable and even higher than the microwire radius and therefore the current

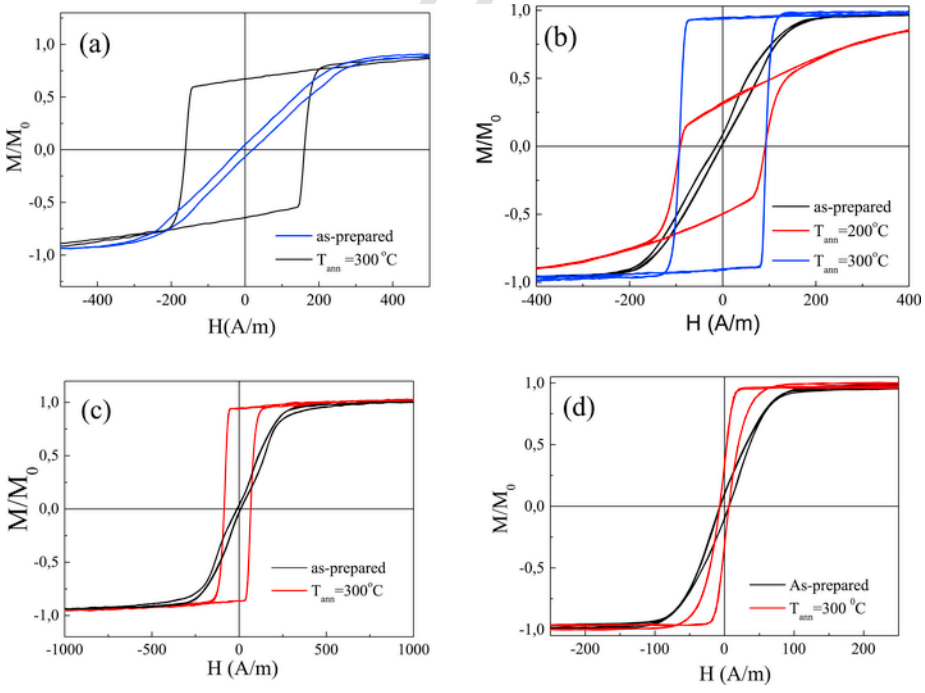

Fig. 9. Effect of annealing on hysteresis loops of $Co_{51}Fe_8Ni_{18}B_{13}Si_{10}$ (a), $Fe_{3\cdot6}Co_{69\cdot2}Ni_1B_{12\cdot5}Si_{11}Mo_{1\cdot5}C_{1.2}$ (b) $Co_{69\cdot2}Fe_{4\cdot1}B_{11\cdot8}Si_{13\cdot8}C_{1.1}$ (c) and $Co_{67}Fe_{3\cdot9}Ni_{1\cdot5}B_{11\cdot5}Si_{14\cdot5}Mo_{1.6}$ (d) microwires.

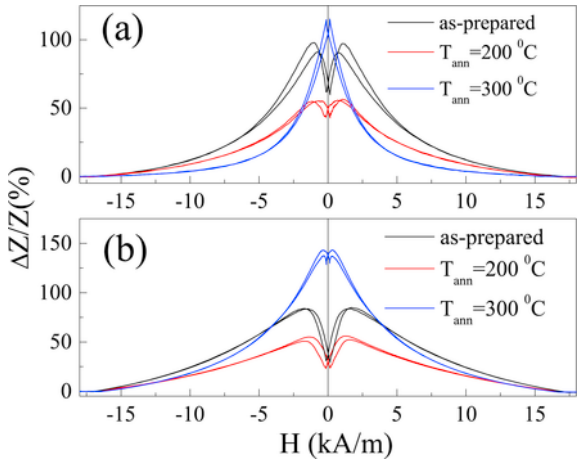

Fig. 10. ΔZ/Z(H) dependencies of as-prepared and annealed at different temperatures $Fe_{3.6}Co_{69.2}Ni_1B_{12.5}Si_{11}Mo_{1.5}C_{1.2}$ microwires measured at 50 MHz (a) and 200 MHz(b).

flows through the whole ferromagnetic nucleus. However, rising the frequency the current flows closer to the surface [7–11,42].

In principle, changes of the magnetic anisotropy upon annealing can be explained considering evaluation of the hysteresis loops and changes of domain structure after annealing (i.e., related to internal stresses relaxation). As commonly accepted, the domain structure of magnetic wires consists of inner axially magnetized core surrounded by the outer shell with transverse magnetization orientation [42,70,75].

The volume of inner axially magnetized core radius, R_c, can be evaluated from the hysteresis loop considering the relation of the squireness ratio, M_r/M_s, and R_c expressed as [76]:

$$R_c = R(M_r/Ms)^{1/2}, \quad (6)$$

where R is the microwire radius.

As can be observed from Fig. 9 (a–c) the M_r/M_s ratio increases rapidly upon annealing. This fact reflects the redistribution of magnetic anisotropy during annealing: in the as-prepared sample, almost the entire volume of the microwire presents transverse magnetic anisotropy. However, we must assume that during annealing, the volume of the internal axially magnetized core increases and, therefore, the annealed microwire has predominantly axial magnetic anisotropy.

Although improvement of $\Delta Z/Z_{max}$ –values (from 90 to 150% at 200 MHz, see Fig. 10 (b)) in $Fe_{3.6}Co_{69.2}Ni_1B_{12.5}Si_{11}Mo_{1.5}C_{1.2}$ microwire annealed at T_{ann}=300 °C is observed, in most cases magnetic hardening upon annealing is associated to degradation of the $\Delta Z/Z_{max}$ –values [42,73,76]. As an example, considerable decrease of $\Delta Z/Z_{max}$ –values upon annealing can be deduced from *ΔZ/Z(H)* dependencies measured in as-prepared and annealed at 300 °C $Co_{67}Fe_{3.9}Ni_{1.5}B_{11.5}Si_{14.5}Mo_{1.6}$ microwires (see Fig. 11). Similarly to $Fe_{3.6}Co_{69.2}Ni_1B_{12.5}Si_{11}Mo_{1.5}C_{1.2}$ microwire, a decrease of H_m-values can be appreciated after annealing.

As can be appreciated from Fig. 12, only $Fe_{3.6}Co_{69.2}Ni_1B_{12.5}Si_{11}Mo_{1.5}C_{1.2}$ microwire annealed at 300 °C presents higher $\Delta Z/Z_{max}$ –values in a wide frequency range. Generally, the optimum frequency range for GMI effect in $Fe_{3.6}Co_{69.2}Ni_1B_{12.5}Si_{11}Mo_{1.5}C_{1.2}$ microwire is between 100 and 200 MHz, while for $Co_{67}Fe_{3.9}Ni_{1.5}B_{11.5}Si_{14.5}Mo_{1.6}$ microwire is between 300 and 400 MHz (see Fig. 12).

As mentioned above, the magnetic field dependence of impedance is determined by magnetic anisotropy features: a decay of

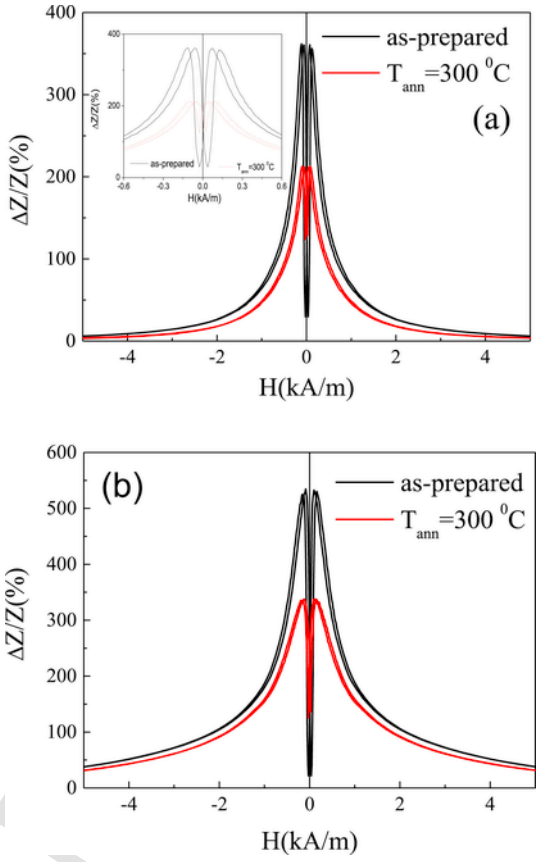

Fig. 11. ΔZ/Z(H) dependencies of as-prepared and annealed at 300 °C $Co_{67}Fe_{3.9}Ni_{1.5}B_{11.5}Si_{14.5}Mo_{1.6}$ microwires measured at 50 MHz (a) and 200 MHz (b).

impedance, Z, versus H is predicted [46] and experimentally observed [42,59] for magnetic wires with axial magnetic anisotropy, while double maximum *Z(H)* dependencies are typically observed for magnetic wires presenting transversal magnetic anisotropy [46,59]. Therefore, in as-prepared sample where almost whole sample volume presents transverse magnetic anisotropy the double-peak *ΔZ/Z(H)* dependence is expected; in the annealed microwires with rectangular hysteresis loops the volume of axially magnetized core is assumed to extend to almost the whole wire diameter. Consequently, as expected a decay of *ΔZ/Z* versus *H* is observed for annealed $Fe_{3.6}Co_{69.2}Ni_1B_{12.5}Si_{11}Mo_{1.5}C_{1.2}$ sample (f=50 MHz). However, double peak *ΔZ/Z(H)* dependencies observed in annealed $Co_{67}Fe_{3.9}Ni_{1.5}B_{11.5}Si_{14.5}Mo_{1.6}$ and $Fe_{3.6}Co_{69.2}Ni_1B_{12.5}Si_{11}Mo_{1.5}C_{1.2}$ (at $f \geq 200$ MHz) microwires can be interpreted considering existence of thin surface layer with transverse magnetic anisotropy even in Co-rich microwires with rectangular hysteresis loops.

Observed transformation of linear hysteresis loops to rectangular upon annealing of Co-rich microwires presents general character: similar behaviour has been reported for large number of Co-rich microwires with vanishing and negative magnetostriction coefficient [42,73–75].

Such annealing influence has been related to internal stresses relaxation as well as to the magnetostriction coefficient modification upon annealing [42,73-76]. As mentioned above, stress annealing is a useful tool, allowing tuning of magnetic anisotropy and improvement of magnetic softness and GMI ratio in microwires [42,73,74]. Therefore, we employed stress-annealing of $Fe_{3.6}Co_{69.2}Ni_1B_{12.5}Si_{11}Mo_{1.5}C_{1.2}$ samples varying annealing temperature, tensile stress applied during the annealing and annealing time.

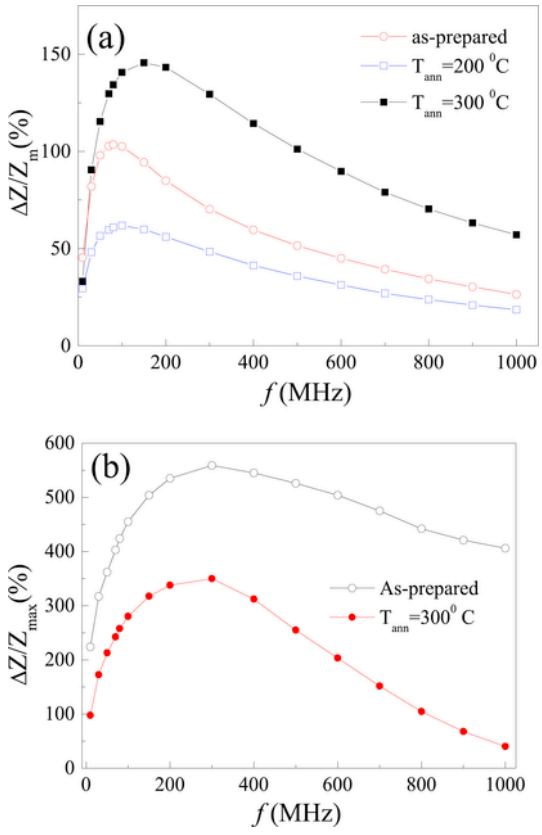

Fig. 12. $\Delta Z/Z\max(f)$ evaluated for as-prepared and annealed at $Tann = 300\,°C$ and $Tann = 200\,°C$ Fe3·6Co69·2Ni1B12·5Si11Mo1·5C1.2 (a) and Co67Fe3·9Ni1·5B11·5Si14·5Mo1.6 (b) microwires.

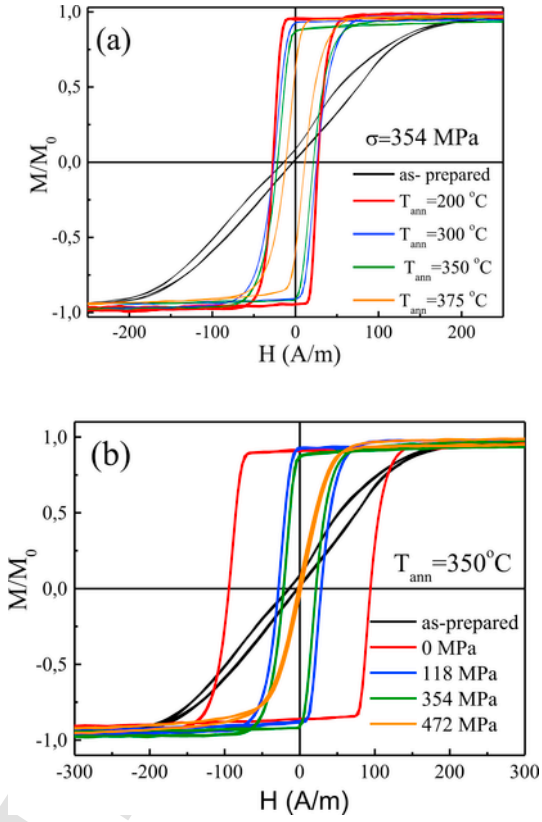

Fig. 13. Hysteresis loops of $Fe_{3\cdot6}Co_{69\cdot2}Ni_1B_{12\cdot5}Si_{11}Mo_{1\cdot5}C_{1.2}$ microwires with stress-annealed at different conditions.

The influence of these parameters on the hysteresis loop of studied microwire is depicted in Fig. 13.

From Fig. 13 we can deduce that indeed, stress-annealing allows manipulation of hysteresis loops and magnetic softness of $Fe_{3\cdot6}Co_{69\cdot2}Ni_1B_{12\cdot5}Si_{11}Mo_{1\cdot5}C_{1.2}$ microwire.

Observed effect of stress-annealing can be summarized as following: i) application of stress during annealing allows remarkable decrease of coercivity and increase of remanent magnetization; ii) both annealing temperature and stress applied during the annealing are essentially relevant iii) increasing either annealing temperature or stress applied during the annealing low coercivity values can be achieved. Accordingly, stress annealing affects the $\Delta Z/Z(H)$ dependencies as well as $\Delta Z/Z_{max}$ -values of studied microwires.

Beneficial influence of stress-annealing on GMI effect of $Fe_{3\cdot6}Co_{69\cdot2}Ni_1B_{12\cdot5}Si_{11}Mo_{1\cdot5}C_{1.2}$ microwire is depicted in Fig. 14. A remarkable GMI ratio improvement upon stress-annealing reflected in an increase of $\Delta Z/Z_{max}$ –values can be underlined from Fig. 14 (a). This GMI ratio improvement is observed for a wide frequency range (see Fig. 14 (b)). In Fig. 14 (b) can be appreciated that the optimum frequency for most of the samples is between 100 and 200 MHz. Moreover, more than 100% increase of $\Delta Z/Z_{max}$ –value (from 100% up to 240%) is achieved by the stress-annealing. Additionally, as-prepared sample presents double-peak $\Delta Z/Z(H)$ dependence (Fig. 14 (a)). However, $\Delta Z/Z(H)$ dependence measured in stress-annealed samples at 200 MHz (Fig. 14 (a)) change from double-peak (observed in as-prepared sample) to almost monotonic decay for stress-annealed microwire ($T_{ann} = 300\,°C$, $\sigma = 236$ MPa).

Observed effect of frequency on $\Delta Z/Z(H)$ dependence can be understood considering aforementioned frequency dependence of the skin penetration depth, δ, as well as magnetic anisotropy distribution within the metallic nucleus.

As discussed elsewhere, the H_m-value corresponding to the peaks (maximum $\Delta Z/Z$ - value) is linked to the average value of the anisotropy field, H_K, at high frequency values, and to the effective anisotropy distribution in the sample [7–11].

As evidenced from Fig. 13, stress annealed microwire presents predominantly axial anisotropy. Therefore, the character of $\Delta Z/Z(H)$ dependence changes from double-peak $\Delta Z/Z(H)$ dependence evident for as-prepared samples to a decay of $\Delta Z/Z$ versus H dependence for stress-annealed samples (Fig. 14 (a)).

The origin of stress-induced anisotropy in amorphous materials [78–80] and particularly in glass-coated microwires [59,81] is previously discussed in terms of either “back stresses” or directional pair (chemical or topological) ordering.

Generally, pair ordering mechanism is assumed for amorphous alloys with two or more magnetic elements. Therefore, in the present case that contains three transition elements, this kind of mechanism can be relevant. However, strong creep anisotropy is recently also reported for glass-coated microwires with only one transition metal [59]. Therefore, we must also consider either back stresses or aforementioned topological short range ordering as the origin of observed creep anisotropy.

Considering the importance of circumferential magnetic permeability for achievement of high GMI effect, recently we have employed Joule heating for GMI effect optimization [32]. We assumed that the circumferential magnetic field, H_{circ}, produced by the current (Oersted field) can affect the magnetic anisotropy of the microwires.

The hysteresis loops of current annealed $Co_{67}Fe_{3\cdot9}Ni_{1\cdot5}B_{11\cdot5}Si_{14\cdot5}Mo_{1.6}$ microwires present extremely

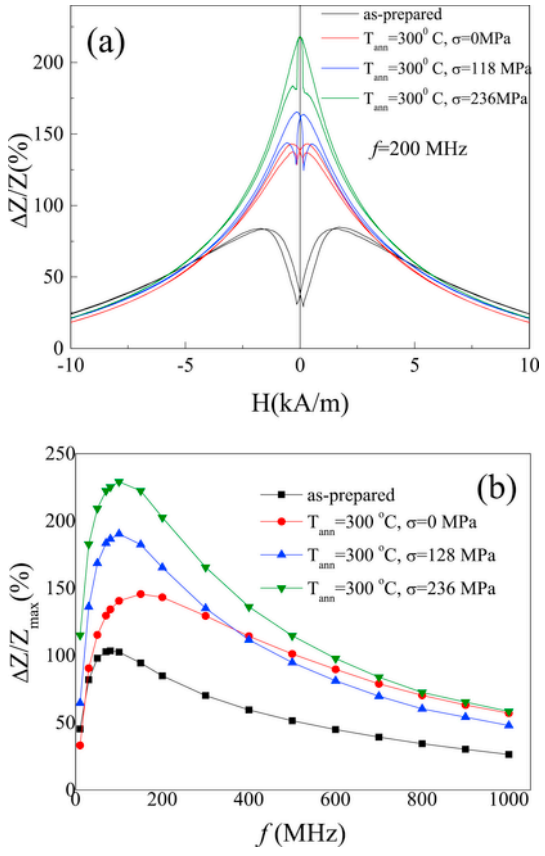

Fig. 14. *ΔZ/Z(H)* dependences of as-prepared and stress-annealed at T_{ann} = 300 °C samples at different σ measured at 200 MHz (a) and $\Delta Z/Z_{max}(f)$ evaluated for as-prepared and annealed at different conditions $Fe_{3\cdot6}Co_{69\cdot2}Ni_1B_{12\cdot5}Si_{11}Mo_{1\cdot5}C_{1.2}$ (b) microwires.

soft magnetic properties: current annealed sample at 40 mA (5 min) present quite low coercivity, H_c, of about 3 A/m (see Fig. 15 (a)). Additionally, from Fig. 15 (a) can be observed that after current annealing studied sample presents lower magnetic anisotropy field, H_k, of about 35 A/m. In contrast to $Co_{67}Fe_{3\cdot9}Ni_{1\cdot5}B_{11\cdot5}Si_{14\cdot5}Mo_{1.6}$ microwire annealed in conventional furnace, Joule heated samples do not exhibit magnetic hardening (see Fig. 15 (b)). For comparison, hysteresis loops of Joule heated and conventionally annealed $Co_{67}Fe_{3\cdot9}Ni_{1\cdot5}B_{11\cdot5}Si_{14\cdot5}Mo_{1.6}$ microwires are presented in Fig. 15 (b). Similar results have been recently reported in Ref. [32].

Consequently, considerable GMI ratio improvement can be observed in Joule heated $Co_{67}Fe_{3\cdot9}Ni_{1\cdot5}B_{11\cdot5}Si_{14\cdot5}Mo_{1.6}$ microwire (see Fig. 15 (c)). This GMI ratio improvement is achieved for a wide frequency range, as can be appreciated from $\Delta Z/Z_{max}(f)$ dependencies provided in Fig. 15 (d).

Summarizing this section on tuning of the GMI effect of Co-rich microwires by post processing, both stress-annealing and Joule heating are promising post-processing methods allowing improvement of GMI effect in Co-rich microwires.

For several years, Fe-rich microwires were not considered as promising giant magnetoimpedance materials due to the predominant axial magnetic anisotropy and, consequently, the low GMI ratio in the as-prepared state. However, relatively high cost of Co and development of novel applications where a large quantity of microwires is needed stimulated development of post-processing method allowing considerable improvement of the GMI effect in Fe-rich microwires.

One of the routes for GMI effect improvement in Fe-rich microwires involves magnetic softening linked to the

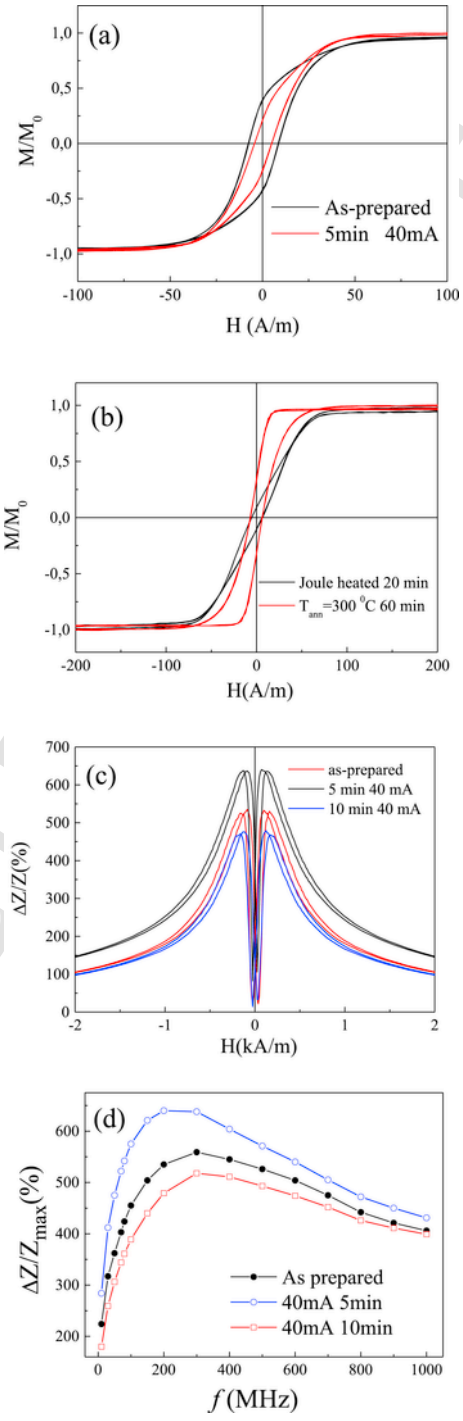

Fig. 15. Hysteresis loops of as-prepared and current annealed at 40 mA for 5 min (a), 30 mA 20 min and at 300 °C for 60 min (b) ΔZ/Z(H) measured at 200 MHz (c) and $\Delta Z/Z_{max}(f)$ (d) dependencies in as-prepared and current annealed at 40 mA for different t_{ann} $Co_{67}Fe_{3\cdot9}Ni_{1\cdot5}B_{11\cdot5}Si_{14\cdot5}Mo_{1.6}$ amorphous glass-coated microwire.

devitrification upon appropriate annealing [19–23]. Magnetic softening of nanocrystalline materials is attributed to their structure consisting of nano-sized grains randomly distributed in an amorphous matrix [14,19–23,82–84]. Such structure achieved in nanocrystalline Fe-SiBNbCu (so-called Finemet) materials is characterized for vanishing magnetocrystalline anisotropy as well as to vanishing magnetostriction coefficient values [14,82–84].

In $Fe_{70.8}Cu_1Nb_{3.1}Si_{14.5}B_{10.6}$ (Finemet-type) microwires (d = 11.2 μm, D = 14.4 μm) the nanocrystallization takes place upon annealing at temperatures of about 500–600 °C (i.e., at temperatures between the first and second crystallization stages) (see Fig. 16 (a)). The microstructure of the devitrified material annealed at appropriate conditions consists of small (below 20 nm average grain size) nanocrystallites embedded in the residual amorphous matrix.

The evolution of structural and magnetic properties is summarized for the $Fe_{70.8}Cu_1Nb_{3.1}Si_{14.5}B_{10.6}$ microwire annealed at different annealing temperatures, T_{ann} (Fig. 16). As-prepared and annealed at $T_{ann} \leq 450$ °C of $Fe_{70.8}Cu_1Nb_{3.1}Si_{14.5}B_{10.6}$ microwires present an amorphous structure. Increasing the T_{ann}, a noticeable growth of the intensity in X-ray diffraction, XRD, patterns is observed, which reveals the beginning of the crystallization upon annealing the sample. Starting from 550 °C, a main crystalline peak appears in the range between 42° and 45°, which corresponds to the existence of α-Fe (Si).

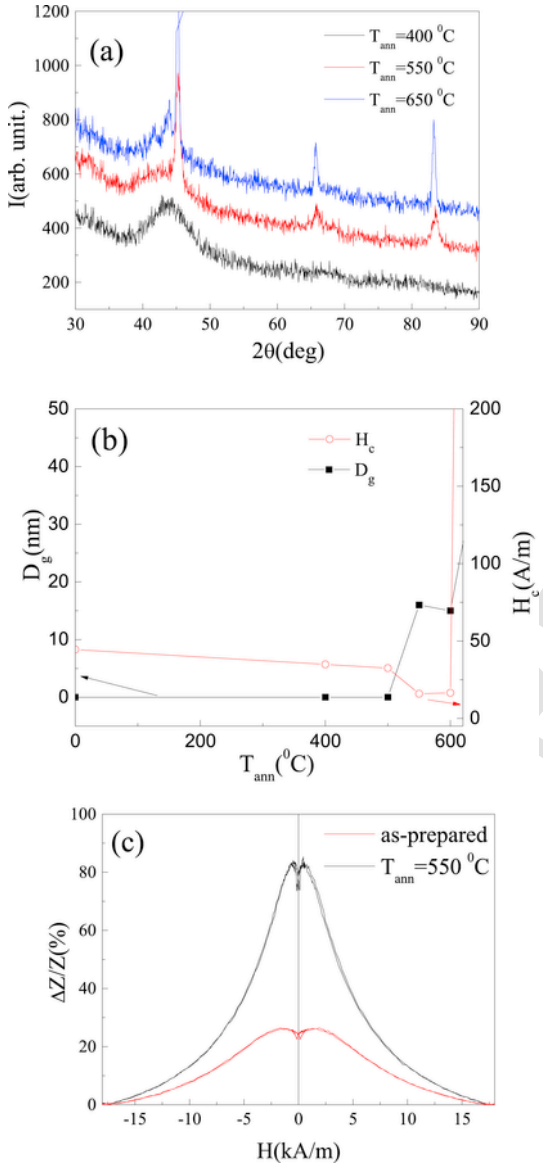

Fig. 16. XRD patterns (a), D_g and H_c dependencies on T_{ann} (b) and $\Delta Z/Z(H)$ dependencies (f = 200 MHz) of as-prepared and annealed at 550 °C (c) $Fe_{70.8}Cu_1Nb_{3.1}Si_{14.5}B_{10.6}$ microwires (ρ = 0.81).

The shape of the peak, particularly its width, contains useful information of the average grain size of the corresponding crystalline phase. Therefore, by estimating the width of the peak, the value of the main grain size, D_g, can be obtained using the Debye-Sherrer equation [82–84]:

$$D_g = k\lambda/\varepsilon \cos 2\theta \quad (6)$$

where, ε is the half width of the crystalline peak and 2θ is the angular position of the maximum crystalline peak.

Correlation of magnetic softening (coercivity decrease) and precipitation of small α-Fe (Si) grains (Fig. 16 (b)) and increasing of the GMI effect upon annealing (Fig. 16 (c)) are observed when the devitrification of amorphous precursor takes place.

Consequently, annealing allowing the devitrification of Finemet-type glass-coated microwires is the effective tool for optimization of magnetic softness and GMI effect of Fe-rich magnetic microwires.

In spite of acceptable magnetic softness and high GMI in devitrified Finemet-type microwires the main disadvantage of such materials is poor mechanical properties [18].

The other possibility to tune the magnetic anisotropy and hence enhance the GMI effect of Fe-rich microwire can be processing by the stress-annealing.

Indeed, stress-annealing of Fe-rich microwires allows appearance of transverse magnetic anisotropy.

After stress annealing of $Fe_{75}B_9Si_{12}C_4$ microwires we observed drastic decreasing of coercivity and remanent magnetization (see Fig. 17).

Consequently, stress-annealed $Fe_{75}B_9Si_{12}C_4$ microwires present considerable enhancement of the GMI effect: rising of maximum GMI ratio (from 5% up to 120%) and change of $\Delta Z/Z(H)$ dependencies from single-peak to double peak (see Fig. 18).

Observed transversal magnetic anisotropy realized in stress-annealed Fe-rich microwires must be attributed to the anisotropies redistribution: increasing of transversal anisotropy at decreasing of axial anisotropy [81].

As can be appreciated from Fig. 19, stress-annealing also allows improvement of the off-diagonal GMI component. S_{21}-values of stress-annealed $Fe_{75}B_9Si_{12}C_4$ microwires measured at Ib = 0 mA become higher (compare with Fig. 8 (b)). Additionally, S_{21}-values of stress-annealed $Fe_{75}B_9Si_{12}C_4$ microwires can be further improved by Ib.

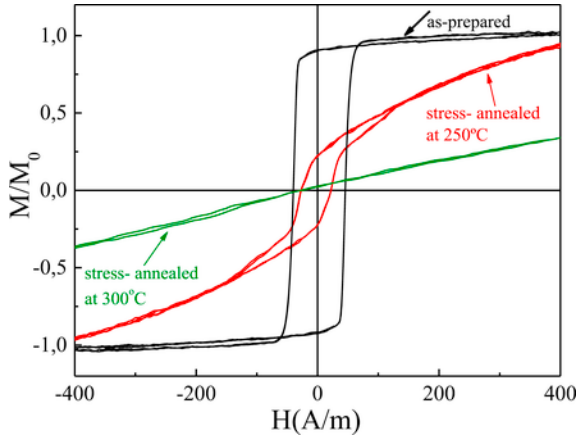

Fig. 17. Hysteresis loops of as-prepared and stress-annealed at different temperatures $Fe_{75}B_9Si_{12}C_4$ microwires.

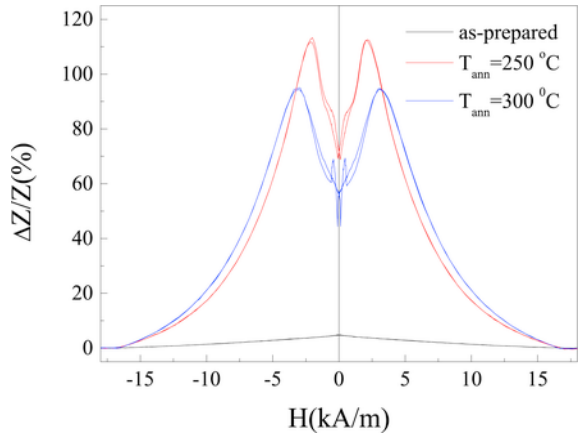

Fig. 18. *ΔZ/Z(H)* dependencies of as-prepared and stress-annealed at different T_{ann} $Fe_{75}B_9Si_{12}C_4$ microwires measured at 200 MHz.

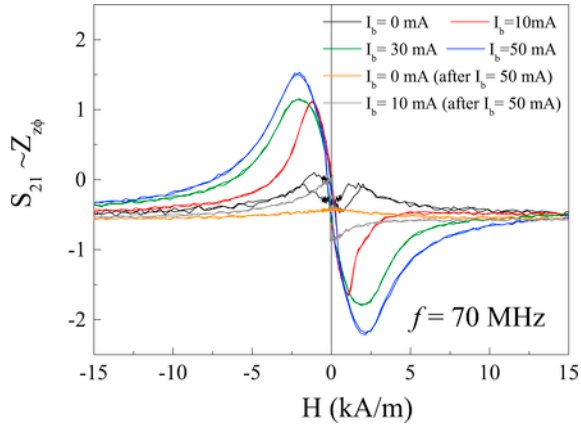

Fig. 19. *$S_{21}(H)$* dependencies measured in stress-annealed $Fe_{75}B_9Si_{12}C_4$ microwires.

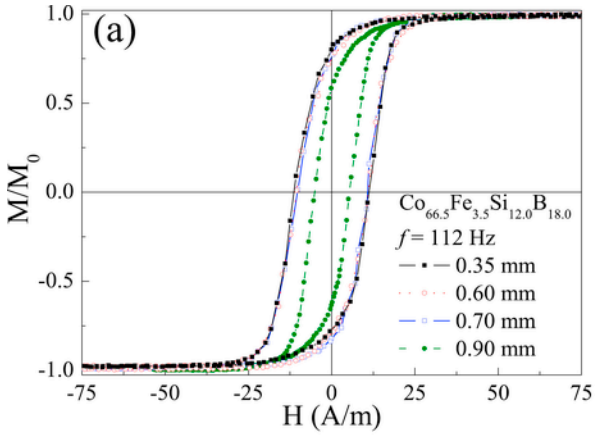

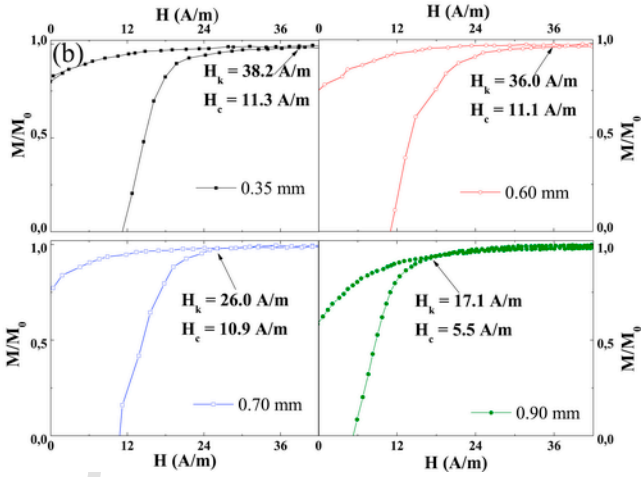

Fig. 20. Normalized axial hysteresis loops (a), and positive part of the hysteresis loops (b), of four $Co_{66.5}Fe_{3.5}Si_{12.0}B_{18.0}$ ribbons with different width. Arrows indicate the anisotropy field for each sample. Reprinted from Ref. [85].

Consequently, we must underline that the stress-annealing is the effective method for tuning of magnetic properties and at certain conditions for improvement of magnetic softness and GMI effect of Fe-rich glass-coated microwires.

3.2. Amorphous ribbons

The other kind of rapidly quenched materials that can present excellent magnetic softness and hence high GMI effect are amorphous ribbons. Below we provide results on GMI effect optimization in soft ferromagnetic Co-rich ($Co_{66.5}Fe_{3.5}Si_{12.0}B_{18.0}$ and $(Co_{0.95}Fe_{0.05})_{75}Si_{10}B_{15}$) amorphous ribbons produced by melt spinning at cooling rates of 10^3–10^6 K/s as described elsewhere [9,14,57].

Thin (width, *w*, from 0.35 to 0.90 mm, thickness from 20 μm) $Co_{66.5}Fe_{3.5}Si_{12.0}B_{18.0}$ amorphous ribbons (with nominal composition and $\lambda_S \sim -0.1\times10^{-6}$) can present excellent magnetic softness: coercivity, H_c, of about 5–10 A/m (see Fig. 20). The effective anisotropy field evaluated from the knee area just before to the approach magnetic saturation, gives quite low values from 17.1 to 40 A/m.

Similarly to magnetic microwires, GMI ratio is considerably affected by the chemical composition as well as by the samples geometry. Thus, $Co_{66.5}Fe_{3.5}Si_{12.0}B_{18.0}$ ribbons width considerably affects *ΔZ/Z(H)* dependencies (see Fig. 21).

As mentioned above, the value of *H* corresponding to the peaks (*Z* maximum value) is linked to the average value of the anisotropy field, H_K, at high frequency values, and to the anisotropy distribution in the sample. In the case of 0.90 mm width ribbon, MI peaks shift to higher magnetic fields. The origin of this shift can be related to the change in skin depth with the frequency-dependent magnetic permeability.

Similarly to magnetic microwires, GMI effect of as-prepared $Co_{66.5}Fe_{3.5}Si_{12.0}B_{18.0}$ ribbons is affected by the ribbons geometry: ribbons with $w=0.7$ mm present quite higher GMI effect (up to 140%, see Fig. 22 (a)). However, ribbons of the same composition with $w=0.6$ mm present lower GMI ratio (see Fig. 22 (b)).

Similarly to magnetic microwires, GMI performance of ribbons can be improved by appropriate annealing (see Fig. 23). In the present case, pre-annealing followed by the stress annealing of $Co_{66.5}Fe_{3.5}Si_{12.0}B_{18.0}$ ribbon (thickness 0.7 mm) is the most effective: such annealing allows improvement of the GMI ratio up to $\Delta Z/Z_m \approx 425\%$ (see Fig. 23 (c)). For as-cast and post-processed ribbons the optimal frequency range is shifted to low frequencies regions (as-compared to microwires): the highest *ΔZ/Z*-values are observed between 30 and 70 MHz (see Figs. 21–24). However, similarly to magnetic microwires, GMI ratio of $(Co_{0.95}Fe_{0.05})_{75}Si_{10}B_{15}$ ribbons can be considerably improved by Joule heating (see Fig. 24).

The off-diagonal MI component, $Z_{\phi z}$, arises from the presence of a non-axial anisotropy. Consequently, as it is shown in Fig. 25 $Z_{\phi z}(H)$ of $Co_{66.5}Fe_{3.5}Si_{12}B_{18}$ ribbon (thickness 20 μm) behaves in a similar way to that reported for Co-rich microwires (see Fig. 8 (a)) displaying two similar branches with different sign according to the

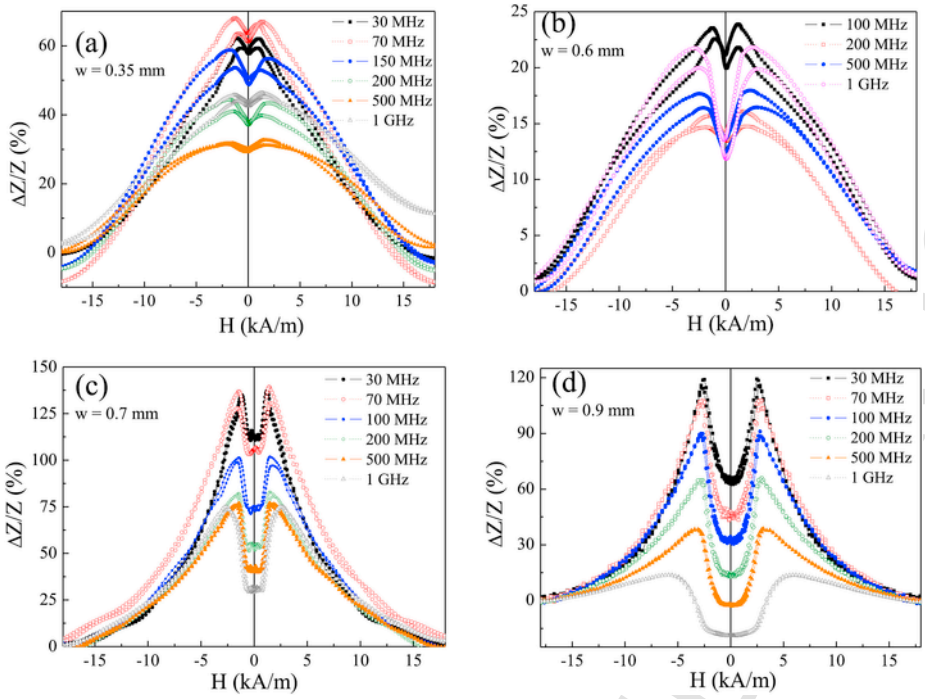

Fig. 21. Impedance of samples with different values of the width: 0.35 mm (a), 0.60 mm (b), 0.70 mm (c), and 0.90 mm (d), as a function of the magnetic field applied in the ribbon direction, for different frequency values in the range 10–1000 MHz [85]. It can be seen that the two-peak behaviour (symmetrically with respect to *H*) emerges more clearly as increasing the frequency (see Figs. 21 and 22).

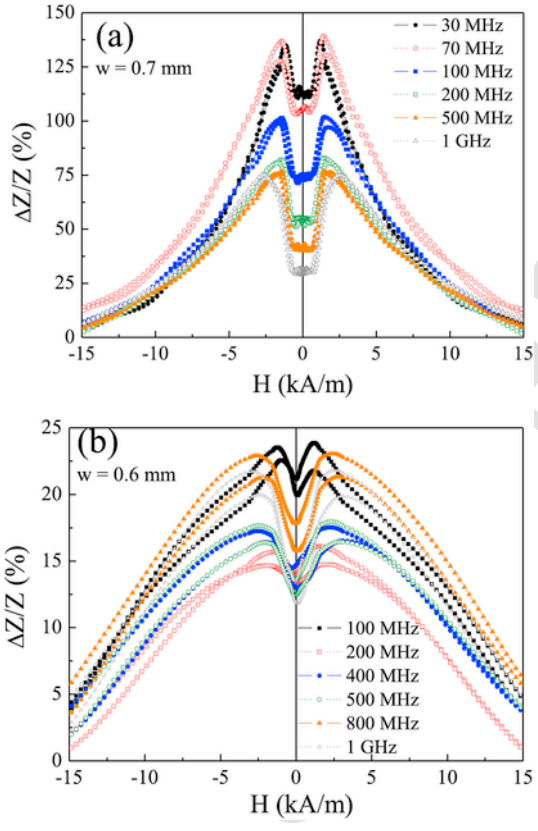

Fig. 22. *ΔZ/Z (H)* dependencies of as-cast $Co_{66.5}Fe_{3.5}Si_{12.0}B_{18.0}$ ribbon of 0.7 mm (a) and 0.6 mm (b) width measured at different frequencies.

direction of the applied magnetic field. Upon influence of bias current, I_b, the $Z_{\phi z}(H)$ dependence considerably changes. When high enough bias current is applied the $Z_{\phi z}(H)$ dependence presents asymmetric character (Fig. 25). Thicker (32 μm thick) as-cast $(Co_{0.95}Fe_{0.05})_{75}Si_{10}B_{15}$ ribbons present relatively low (about 80%) GMI ratio (see Fig. 24 (a)).

Stress–annealed $Co_{66.5}Fe_{3.5}Si_{12}B_{18}$ ribbons present much lower and irregular $Z_{\phi z}$ if no dc bias current, I_b, is applied (see Fig. 26). However, the off-diagonal response significantly increases upon bias current application and becomes antisymmetric with respect to the field *H*, having almost linear behaviour in the field range of 400 A/m, for most of stress-annealed samples (see Fig. 26).

This behaviour can be attributed to the influence of the transverse dc field created by the bias current, which makes one of the opposite (depending on the current direction) transverse magnetization direction more favourable. Domains with magnetization lying along the bias field increase at the expense of domains with magnetization aligned against this field. If the transverse magnetic field is sufficiently high, the field dependence of the off-diagonal impedance becomes asymmetric as it is shown in Fig. 26.

In fact, similarly to magnetic microwires Joule heating can considerably affect the $\Delta Z/Z_{max}$-value and *ΔZ/Z(H)* dependencies and improve high-frequency GMI effect (Fig. 27). Similarly to magnetic microwires magnetic field, GMI ratio improvement can be linked to transverse induced magnetic anisotropy related with the magnetic field produced by the current (Oersted field).

Consequently, from provided results we must conclude that the most common way to optimize the GMI effect in magnetic microwires and ribbons is preparation of amorphous materials with nearly-zero magnetostriction coefficient. Accordingly, quite high GMI ratio has been reported for as-prepared Co-rich microwires (up to about 600%) and ribbons (up to 140%) with appropriate chemical composition (vanishing λ_s - values).

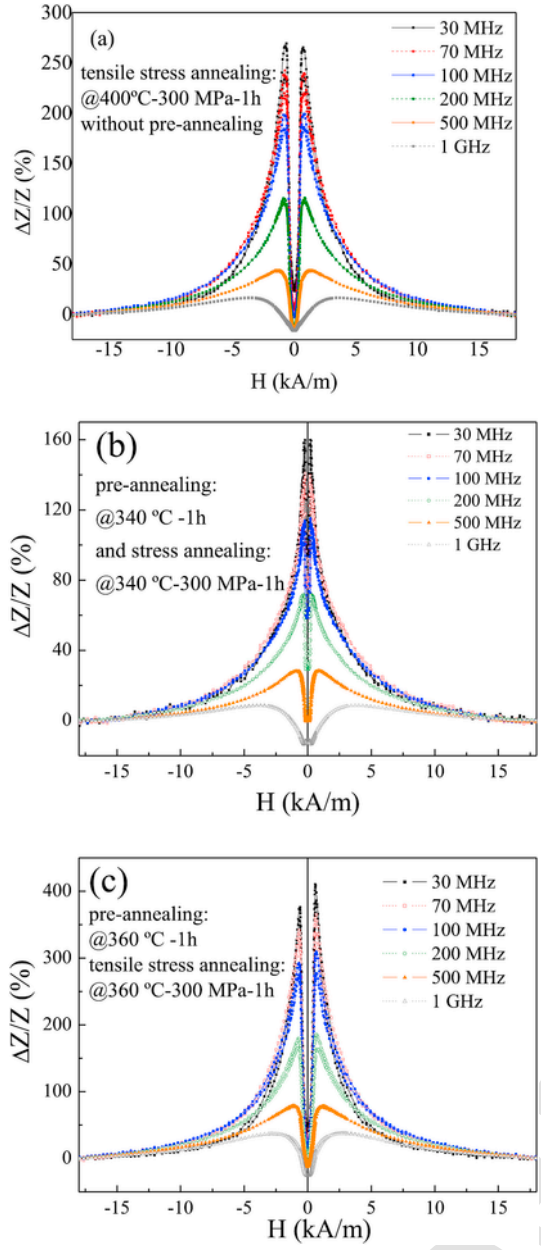

Fig. 23. *ΔZ/Z (H)* dependencies of annealed $Co_{66.5}Fe_{3.5}Si_{12.0}B_{18.0}$ ribbon (thickness 0.7 mm) measured in the range 10–1000 MHz.

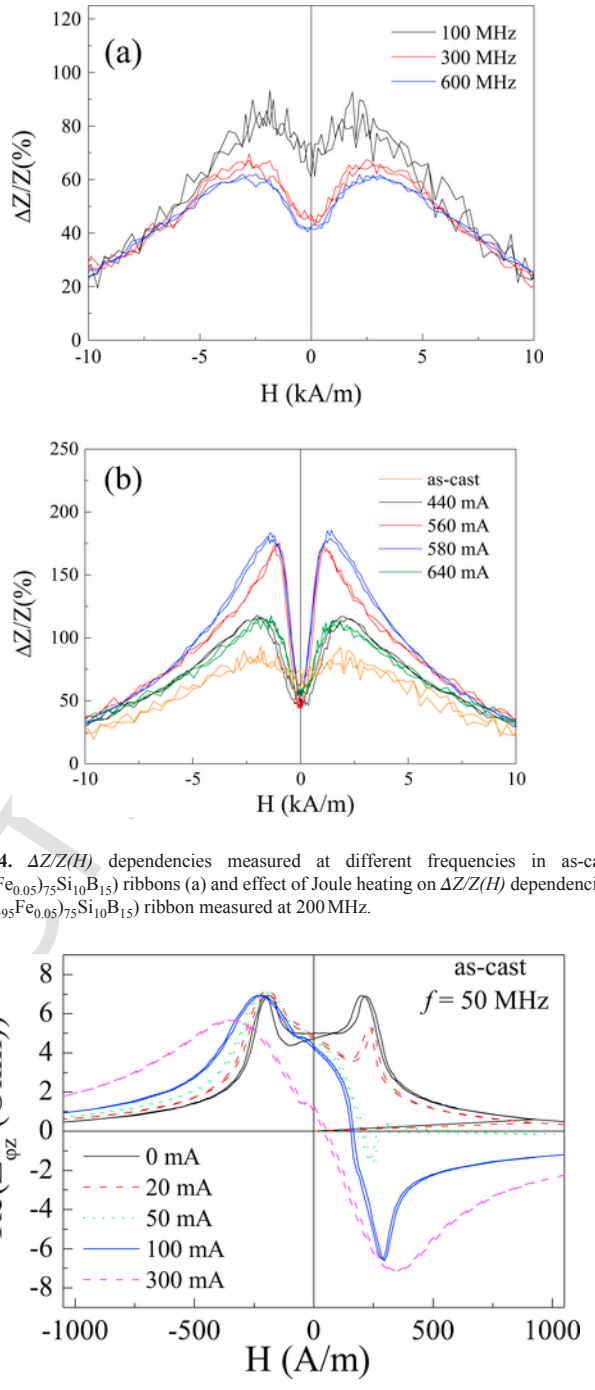

Fig. 24. *ΔZ/Z(H)* dependencies measured at different frequencies in as-cast $(Co_{0.95}Fe_{0.05})_{75}Si_{10}B_{15}$) ribbons (a) and effect of Joule heating on *ΔZ/Z(H)* dependencies of $(Co_{0.95}Fe_{0.05})_{75}Si_{10}B_{15}$) ribbon measured at 200 MHz.

Fig. 25. Magnetic field dependence of the off-diagonal impedance component of the as-cast $Co_{66.5}Fe_{3.5}Si_{12}B_{18}$ amorphous ribbon measured at different I_b -values.

It is worth mentioning that the highest GMI ratios are reported for magnetic microwires [30–32]. However, GMI materials are not limited by microwires and ribbons: high GMI ratios have been reported for various soft magnetic materials, like amorphous, i.e., in-rotating water quenched wires [87], melt extracted wires [88], nanocrystalline microwires [23], in-rotating quenched devitrified wires [89] and thin films [24,25]. The comparison summarizing the previous achievements on GMI effect of magnetic materials is provided in Table 2.

As can be appreciated from provided above comparison of the previous achievements on GMI effect, the highest GMI ratios are achieved for rapidly quenched materials with either amorphous or nanocrystalline structure. Additionally, the appropriate post-processing is a useful tool for GMI effect optimization. Accordingly, a number of recent publications have been reported on the development of high-performance magnetic sensors using rapidly quenching materials [91–93].

4. Conclusions

Magnetic microwires and ribbons present high GMI effect adjustable through the preparation process and post-production processing such as various types of annealing (furnace, Joule heating, field-annealing, stress-annealing). We overviewed the influence of preparation conditions and possibility to control the magnetic properties

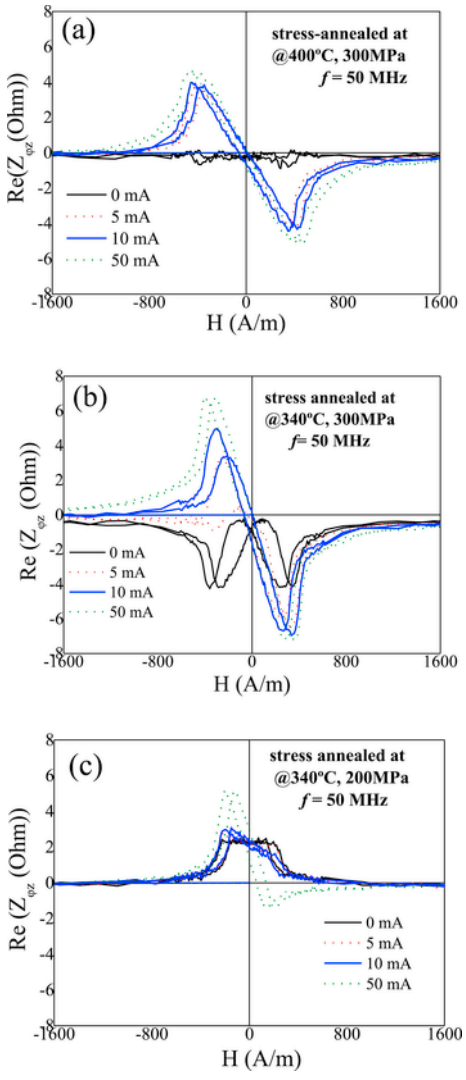

Fig. 26. Off-diagonal impedance component of the stress-annealed $Co_{66.5}Fe_{3.5}Si_{12}B_{18}$ ribbons measured at different I_b-values.

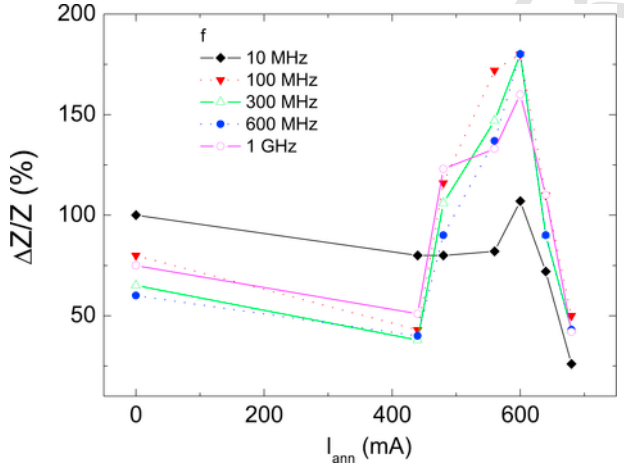

Fig. 27. Frequency dependence of the maximal GMI effect $\Delta Z/Z$ as a function of annealing current $I_{ann.}$ [86].

Table 2
Summary of the previous literatures on Giant Magneto-Impedance effect of magnetic materials.

Magnetic materials/preparation method	Maximum GMI ratio, $\Delta Z/Z_{max}$ (%)	Source
Crystalline, mumetal wire/annealed	40	[6]
Amorphous, Co-rich wire/in-rotating water	350	[87]
Amorphous, Co-rich wire/melt extracted	450	[88]
Thin films Co-rich/sputtered, filed annealed	40	[24]
Amorphous Co-rich, glass-coated microwire/ Taylor-Ulitovsky, Joule heated	600	[31]
Amorphous Co-rich, glass-coated microwire/ Taylor-Ulitovsky, as-prepared	615	[30]
Amorphous Co-rich, glass-coated microwire/ Taylor-Ulitovsky, Joule heated	650	[32]
Nanocrystalline Fe-rich wires/in-rotating water, annealed	120	[89]
Nanocrystalline Fe-rich,glass-coated microwire/Taylor-Ulitovsky, annealed	125	[23]
Amorphous Fe–Ni rich glass-coated microwire/Taylor-Ulitovsky, annealed	45	[90]
Amorphous Fe-rich glass-coated microwire/ Taylor-Ulitovsky, as-prepared	30	[69]
Amorphous Fe-rich glass-coated microwire/ Taylor-Ulitovsky, stress-annealed	125	[59,69]
Nanocrystalline ribbon prepared by appropriate annealing	640	[33]

of amorphous ferromagnetic microwires and ribbons by the annealing. As-prepared Co-rich microwires and ribbons can present low coercivity and high GMI effect, while the magnetoelastic anisotropy determines the magnetic softness and GMI effect of glass-coated microwires. We demonstrated that annealing conditions drastically affect the magnetic properties. We observed transformation of inclined hysteresis loops to rectangular and GMI effect improvement in amorphous Co-rich microwire after annealing. The opposite tendency: transformation of rectangular hysteresis loops to linear and drastic increasing of GMI effect is observed in Fe-rich microwires after stress-annealing. The observed dependencies are attributed to stress relaxation and changes in the magnetostriction after sample annealing as well as the internal stresses redistribution after stress-annealing. Stress-annealing and Joule heating allow optimization of GMI effect in both microwires and ribbons. Magnetic softening observed after annealing of Finemet-type glass-coated microwires in the range between 400°C and 650 °C is explained in terms of the devitrification process caused by nanocrystallization. Enhancement of GMI observed upon annealing asserts the optimum magnetic softness of the Finemet-type glass-coated microwires after devitrification.

[28][77].

Acknowledgements

This work was supported by Spanish MCIU under PGC2018-099530-B-C31 (MCIU/AEI/FEDER, UE), by the Government of the Basque Country under PIBA 2018–44 and under Elkartek RTM 4.0 projects, by Russian Foundation for Basic Research (Grant 16-53-48012) and partially supported by Act 211 Government of the Russian Federation, contract # 02. A03.21.0011. The authors thank for technical and human support provided by SGIker of UPV/EHU and European funding (ERDF and ESF). The work was carried out with financial support from the Ministry of Education and Science of the Russian Federation in the framework of increase Competitiveness Program of NUST "MISIS", implemented by a governmental decree dated 16th of March 2013, No 211.

References

[1] J.M.D. Coey, Magnetism, Magnetic Materials, The Edinburgh Building, Cambridge University Press, Cambridge CB2 8RU, UK, 2009p.614, 13 978-0-521-81614-4.

[2] Novel Functional Magnetic Materials, Springer international publishing, in: Applications Fundamentals, A. Zhukov (Eds.), Springer Ser. Mater. Sci. 231 (2016) https://doi.org/10.1007/978-3-319-26106-5, 0933–033X.

[3] F. Fiorillo, G. Bertotti, C. Appino, M. Pasquale, Soft Magnetic Materials, J. Webster (Eds.), Wiley Encyclopedia of Electrical and Electronics Engineering, John Wiley & Sons, Inc., p.42, 1999https://doi.org/10.1002/047134608X.W4504.pub2.

[4] D.C. Jiles, Recent advances and future directions in magnetic materials, Acta Mater. 51 (2003) 5907–5939.

5. High Performance Soft Magnetic Materials, In: A. Zhukov (Ed.), Springer Series in Materials Science, 252, Springer International Publishing, 2017, p. 216, https://doi.org/10.1007/978-3-319-49707-5, 0933-033X.

[6] E.P. Harrison, G.L. Turney, H. Rowe, Electrical properties of wires of high permeability, Nature 135 (1935) 961.

[7] M. Knobel, M. Vazquez, L. Kraus, Giant magnetoimpedance, Handbook of magnetic materials ed. E., Brucke 15 (2003) 497–563.

[8] A. Zhukov, M. Ipatov, V. Zhukova, Advances in giant magnetoimpedance of materials, handbook of magnetic materials, in: K.H.J. (Ed.), Buschow 24 (2015) 139–236, ch.2.

[9] V.E. Makhotkin, B.P. Shurukhin, V.A. Lopatin, P.Y. Marchakov, Y.K. Levin, Magnetic field sensors based on amorphous ribbons, sens, Actuators 21 (1991) 759–762.

[10] L.V. Panina, K. Mohri, Magneto-impedance effect in amorphous wires, Appl. Phys. Lett. 65 (1994) 1189–1191.

[11] R. Beach, A. Berkowitz, Giant magnetic field dependent impedance of amorphous FeCoSiB wire, Appl. Phys. Lett. 64 (1994) 3652–3654.

[12] I.S. Miroshnichenko, I.V. Salli, A device for the crystallization of alloys at a high cooling rate, Ind. Lab. 25 (1959) 1463–1464, in English, Zav. Lab., 25 (1959) 1398.

[13] P. Duwez, R.J. Williams, K.J. Klement, Continuous series of metastable solid solutions in Ag-Cu alloys, J. Appl. Phys. 31 (1966) 1136–1142.

[14] G. Herzer, Amorphous and nanocrystalline soft magnets, in: George C. Hadjipanayis (Ed.), Proceedings of the NATO Advanced Study Insititute on Magnetic Hysteresis in Novel Materials, Mykonos, Greece, 1-12 July 1996, vol. 338, Kluwer Academic Publishers, Dordrecht/Boston/London, 1997, pp. 711–730, NATO ASI Series (Series E: Applied Sciences).

[15] M. Hagiwara, A. Inoue, T. Masumoto, Mechanical properties of Fe–Si–B amorphous wires produced by in-rotating-water spinning method, Metall. Trans. 13A (1982) 373–382.

[16] P. Rudkowski, G. Rudkowska, J.O. Strom-Olsen, The fabrication of fine metallic fibers by continuous melt extraction and their magnetic and mechanical properties, Mater. Sci. Eng. A 133 (1991) 158–161.

[17] T. Goto, M. Nagano, N. Wehara, Mechanical properties of amorphous $Fe_{80}P_{16}C_3B_1$ filament produced by glass-coated melt spinning, Trans. JIM 18 (1977) 759–764.

[18] V. Zhukova, A.F. Cobeño, A. Zhukov, A.R. de Arellano Lopez, S. López-Pombero, J.M. Blanco, V. Larin, J. Gonzalez, Correlation between magnetic and mechanical properties of devitrified glass-coated $Fe_{71.8}Cu_1Nb_{3.1}Si_{15}B_{9.1}$ microwires, J. Magn. Magn. Mater. 249 (2002) 79–84, P1-II.

[19] M.E. McHenry, M.A. Willard, D.E. Laughlin, Amorphous and nanocrystalline materials for applications as soft magnets, Prog. Mater. Sci. 44 (1999) 291–433.

[20] H.Q. Guo, H. Kronmüller, T. Dragon, Z.H. Cheng, B.G. Shen, Influence of nanocrystallization on the evolution of domain patterns and the magnetoimpedance effect in amorphous $Fe_{73.5}Cu_1Nb_3Si_{13.5}B_9$ ribbons, J. Appl. Phys. 89 (2001) 514–520.

[21] A.P. Zhukov, A. Talaat, M. Ipatov, J.M. Blanco, L. Gonzalez-Legarreta, B. Hernando, V. Zhukova, Effect of nanocrystallization on magnetic properties and GMI effect of microwires, IEEE Trans. Magn. 50 (6) (2014) 2501905.

[22] H. Chiriac, T.A. Ovari, C.S. Marinescu, Giant magneto-impedance effect in nanocrystalline glass-covered wires, J. Appl. Phys. 83 (1998) 6584–6586.

[23] A. Talaat, V. Zhukova, M. Ipatov, J.J. del Val, J.M. Blanco, L. Gonzalez-Legarreta, B. Hernando, M. Churyukanova, A. Zhukov, Engineering of magnetic softness and magnetoimpedance in Fe-rich microwires by nanocrystallization, J. Occup. Med. 68 (6) (2016) 1563–1571.

[24] L.V. Panina, K. Mohri, T. Uchyama, M. Noda, Giant magneto-impedance in Co-rich amorphous wires and films, IEEE trans. Magn. 31, NOVAcura 2 (1995) 1249–1260.

[25] H. Kikuchi, C. Sumida, Analysis of asymmetric property with DC bias current on thin-film magnetoimpedance element, AIP Adv. 8 (2018) 056618.

[26] C. García, J.M. Florez, P. Vargas, C.A. Ross, Asymmetrical giant magnetoimpedance in exchange-biased NiFe, Appl. Phys. Lett. 96 (2010) 232501.

[27] D. Karnaushenko, D.D. Karnaushenko, D. Makarov, S. Baunack, R. Schäfer, O.G. Schmidt, Self-assembled on-chip-integrated giant magneto-impedance sensorics, Adv. Mater. 27 (2015) 6582–6589.

[28] R.B. da Silva, A.D.C. Viegas, V.P. Nascimento, M.A. Corrêa, L.F. Schelp, E. Baggio-Saitovitch, R.L. Sommer, High frequency magnetoimpedance in $Ni_{81}Fe_{19}/Fe_{50}Mn_{50}$ exchange biased multilayer, Appl. Phys. Lett. 94 (2009) 042501.

[29] M. Coïsson, G. Barrera, F. Celegato, P. Tiberto, F. Vinai, Soft magnetic thin films: influence of annealing on magnetic properties, J. Phys. Conf. Ser. 365 (2012) 012003.

[30] A. Zhukov, V. Zhukova, J.M. Blanco, J. Gonzalez, Recent research on magnetic properties of glass-coated microwires, J. Magn. Magn. Mater. 294 (2005) 182–192.

[31] K.R. Pirota, L. Kraus, H. Chiriac, M. Knobel, Magnetic properties and GMI in a CoFeSiB glass-covered microwire, J. Magn. Magn. Mater. 21 (2000) L243–L247.

[32] P. Corte-León, V. Zhukova, M. Ipatov, J.M. Blanco, J. Gonzalez, A. Zhukov, Engineering of magnetic properties of Co-rich microwires by joule heating, Intermetallics 105 (2019) 92–98.

[33] M.-H. Phan, H.-X. Peng, S.-C. Yu, M. Vázquez, Optimized giant magnetoimpedance effect in amorphous and nanocrystalline materials, J. Appl. Phys. 99 (2006), 08C505.

[34] K. Mohri, T. Uchiyama, L.P. Shen, C.M. Cai, L.V. Panina, Amorphous wire and CMOS IC-based sensitive micro-magnetic sensors (MI sensor and SI sensor) for intelligent measurements and controls, J. Magn. Magn. Mater. 249 (2002) 351–356.

[35] Y. Honkura, Development of amorphous wire type MI sensors for automobile use, J. Magn. Magn. Mater. 249 (2002) 375–381.

[36] S. Gudoshnikov, N. Usov, A. Nozdrin, M. Ipatov, A. Zhukov, V. Zhukova, Highly sensitive magnetometer based on the off-diagonal GMI effect in Co-rich glass-coated microwire, Phys. Status Solidi 211 (5) (2014) 980–985.

[37] T. Uchiyama, K. Mohri, Sh Nakayama, Measurement of spontaneous oscillatory magnetic field of Guinea-pig smooth muscle preparation using pico-tesla resolution amorphous wire magneto-impedance sensor, IEEE Trans. Magn. 47 (2011) 3070–3073.

[38] A.F. Cobeño, A. Zhukov, J.M. Blanco, V. Larin, J. Gonzalez, Magnetoelastic sensor based on GMI of amorphous microwire, Sens. Actuators 91 (2001) 95–98.

[39] L. Ding, S. Saez, C. Dolabdjian, L.G.C. Melo, A. Yelon, D. Ménard, Development of a high sensitivity Giant Magneto-Impedance magnetometer: comparison with a commercial Flux-Gate, IEEE Sensors 9 (2) (2009) 159–168.

[40] L. Kraus, Theory of giant magneto-impedance in the planar conductor with uniaxial magnetic anisotropy, J. Magn. Magn. Mater. 195 (1999) 764–778.

[41] M. Ipatov, V. Zhukova, A. Zhukov, J. Gonzalez, A. Zvezdin, Low-field hysteresis in the magnetoimpedance of amorphous microwires, Phys. Rev. B 81 (2010) 134421.

[42] A. Zhukov, M. Ipatov, M. Churyukanova, A. Talaat, J.M. Blanco, V. Zhukova, Trends in optimization of giant magnetoimpedance effect in amorphous and nanocrystalline materials, J. Alloy. Comp. 727 (2017) 887–901.

[43] J. Chen, J. Li, Y. Li, Y. Chen, L. Xu, Design and fabrication of a miniaturized GMI magnetic sensor based on amorphous wire by MEMS technology, Sensors 18 (2018) 732.

[44] Y. Honkura, S. Honkura, The development of ASIC type GSR sensor driven by GHz pulse current, proceedings of the ninth international conference on sensor device technologies and applications, SENSORDEVICES 2018, IARIA (2018) 15–22, 978-1-61208-660-6.

[45] K. Mohri, T. Uchiyama, L.V. Panina, M. Yamamoto, K. Bushida, Recent advances of amorphous wire CMOS IC magneto-impedance sensors: innovative high-performance micromagnetic sensor chip, Journal of Sensors (2015) https://doi.org/10.1155/2015/718069, Article ID 718069.

[46] N.A. Usov, A.S. Antonov, A.N. Lagar'kov, Theory of giant magneto-impedance effect in amorphous wires with different types of magnetic anisotropy, J. Magn. Magn. Mater. 185 (1998) 159–173.

[47] H. Chiriac, N. Lupu, G. Stoian, G. Ababei, S. Corodeanu, T.-A. Óvári Ultrathin, Nanocrystalline magnetic wires, Crystals 7 (2017) 48.

[48] A.P. Zhukov, M. Vázquez, J. Velázquez, H. Chiriac, V. Larin, The remagnetization process of thin and ultrathin Fe-rich amorphous wires, J. Magn. Magn. Mater. 151 (1995) 132–138.

[49] I. Ogasawara, S. Ueno, Preparation and properties of amorphous wires, IEEE Trans. Magn. 31 (2) (1995) 1219–1223.

[50] A. Talaat, J. Alonso, V. Zhukova, E. Garaio, J.A. García, H. Srikanth, M.H. Phan, A. Zhukov, Ferromagnetic glass-coated microwires with good heating properties for magnetic hyperthermia, Sci. Rep. 6 (2016) 39300.

[51] A.V. Ulitovsky, I.M. Maianski, A.I. Avramenco, Method of Continuous Casting of Glass Coated Microwire, Patent No128427 (USSR), 15.05.60, Bulletin, No10, p.14.

[52] R. Gemperle, L. Kraus, J. Schneider, Magnetization reversal in amorphous $(Fe_{1-x}Ni_x)_{80}P_{10}B_{10}$ microwires, Czezh. J. Phys. B 28 (1978) 1138–1145.

[53] S.A. Baranov, V.S. Larin, A.V. Torcunov, Technology, preparation and properties of the cast glass-coated magnetic microwires, Crystals 7 (2017) 136.

[54] H. Chiriac, T.A. Óvári, Amorphous glass-covered magnetic wires: preparation, properties, applications, Prog. Mater. Sci. 40 (5) (1996) 333–407.

[55] A. Zhukov, J. Gonzalez, A. Torcunov, E. Pina, M.J. Prieto, A.F. Cobeño, J.M. Blanco, V. Larin, S. Baranov, Ferromagnetic resonance and structure of Fe-based glass-coated microwires, J. Magn. Magn. Mater. 203 (1999) 238–240.

[56] A. Zhukov, E. Kostitcyna, E. Shuvaeva, S. Kaloshkin, M. Churyukanova, V. Sudarchikova, A. Talaat, V. Zhukova, Effect of composite origin on magnetic properties of glass-coated microwires, Intermetallics 44 (2014) 88–93.

[57] L. González-Legarreta, V.M. Prida, A. Talaat, M. Ipatov, V. Zhukova, A. Zhukov, L.I. Escoda, J.J. Suñol, J. González, B. Hernando, In: Tailoring of Soft Magnetic Properties and High Frequency Giant Magnetoimpedance in Amorphous Ribbons" in High Performance Soft Magnetic Materials (Editor A. Zhukov), Springer Series in Materials Science, vol. 252, Springer International Publishing, 2017, pp. 33–52, https://doi.org/10.1007/978-3-319-49707-5, 0933-033X.

[58] A. Zhukov, A. Talaat, M. Ipatov, V. Zhukova, Tailoring of high frequency giant magnetoimpedance effect of amorphous Co-rich microwires, IEEE Magn. Lett. 6 (2015) 2500104.

[59] V. Zhukova, J.M. Blanco, M. Ipatov, M. Churyukanova, S. Taskaev, A. Zhukov, Tailoring of magnetoimpedance effect and magnetic softness of Fe-rich glass-coated microwires by stress- annealing, Sci. Rep. 8 (2018) 3202.

[60] K. Narita, J. Yamasaki, H. Fukunaga, Measurement of magnetostriction of a thin amorphous ribbon by means of small-angle magnetization rotation, IEEE Trans. Magn. Mag. 16 (1980) 435–439.

[61] A. Zhukov, M. Churyukanova, S. Kaloshkin, V. Sudarchikova, S. Gudoshnikov, M. Ipatov, A. Talaat, J.M. Blanco, V. Zhukova, Magnetostriction of Co-Fe-based amorphous soft magnetic microwires, J. Electron. Mater. 45 (1) (2016) 226–234.

[62] Y. Konno, K. Mohri, Magnetostriction measurements for amorphous wires, IEEE Trans. Magn. 25 (1989) 3623–3625.

[63] K. Mohri, F.B. Humphrey, K. Kawashima, K. Kimura, M. Muzutani, Large barkhausen and matteucci effects in FeCoSiB, FeCrSiB, and FeNiSiB amorphous wires, IEEE Trans. Magn. 26 (1990), 1789–1781.

[64] V. Zhukova, A. Chizhik, A. Zhukov, A. Torcunov, V. Larin, J. Gonzalez, Optimization of giant magneto-impedance in Co-rich amorphous microwires, IEEE Trans. Magn. 38 (2002) 3090–3092, 5, part I.

[65] H. Chiriac, T.-A.- Ovari, A. Zhukov, Magnetoelastic anisotropy of amorphous microwires, J. Magn. Magn. Mater. 254–255 (2003) 469–471.

[66] A.S. Antonov, V.T. Borisov, O.V. Borisov, A.F. Prokoshin, N.A. Usov, Residual quenching stresses in glass-coated amorphous ferromagnetic microwires, J. Phys. D Appl. Phys. 33 (2000) 1161–1168.

[67] J. Velázquez, M. Vazquez, A. Zhukov, Magnetoelastic anisotropy distribution in glass-coated microwires, J. Mater. Res. 11 No 10 (1996) 2499–2505.

[68] D. Ménard, M. Britel, P. Ciureanu, A. Yelon, Giant magnetoimpedance in a cylindrical conductor, J. Appl. Phys. 84 (1998) 2805–2814.

[69] V. Zhukova, J.M. Blanco, M. Ipatov, J. Gonzalez, M. Churyukanova A., Zhukov, Engineering of magnetic softness and giant magnetoimpedance effect in Fe-rich microwires by stress-annealing, Scr. Mater. 142 (2018) 10–14, https://doi.org/10.1016/j.scriptamat.2017.08.014.

[70] M. Ipatov, V. Zhukova, J. Gonzalez, A. Zhukov, Magnetoimpedance hysteresis in amorphous microwires induced by core–shell interaction, Appl. Phys. Lett. 105 (2014) 122401.

[71] V. Zhukova, A.F. Cobeño, A. Zhukov, J.M. Blanco, S. Puerta, J. González, M. Vázquez, Tailoring of magnetic properties of glass coated microwires by current annealing, J. Non-Cryst. Solids 287 (2001) 31–36.

[72] R.G. Eggert, Minerals go critical, Nat. Chem. 3 (2011) 688–691.

[73] A. Zhukov, A. Talaat, M. Ipatov, J.M. Blanco, V. Zhukova, Tailoring of magnetic properties and GMI effect of Co-rich amorphous microwires by heat treatment, J. Alloy. Comp. 615 (2014) 610–615.

[74] A. Zhukov, K. Chichay, A. Talaat, V. Rodionova, J.M. Blanco, M. Ipatov, V. Zhukova, Manipulation of magnetic properties of glass-coated microwires by annealing, J. Magn. Magn. Mater. 383 (2015) 232–236.

[75] V. Zhukova, J.M. Blanco, M. Ipatov, A. Zhukov, Effect of transverse magnetic field on domain wall propagation in magnetically bistable glass-coated amorphous microwires, J. Appl. Phys. 106 (2009) 113914.

[76] M. Vázquez, D.-X. Chen, The magnetization reversal process in amorphous wires,, IEEE Trans. Magn. 31 (2) (1995) 1229–1239.

[77] A. Zhukov, A. Talaat, M. Churyukanova, S. Kaloshkin, V. Semenkova, M. Ipatov, J.M. Blanco, V. Zhukova, Engineering of magnetic properties and GMI effect in Co-rich amorphous microwires, J. Alloy. Comp. 664 (15) (2016) 235–241.

[78] J. González, M. Vázquez, J.M. Barandiarán, V. Madurga, A. Hernando, Different kinds of magnetic anisotropies induced by current annealing in metallic glasses, J. Magn. Magn. Mater. 68 (1987) 151–156.

[79] F.E. Luborsky, J.L. Walter, Magnetic anneal anisotropy in amorphous alloys, IEEE Trans.Magn., 13, No 2 (1977) 953–956.

[80] J. Haimovich, T. Jagielinski, T. Egami, Magnetic and structural effects of anelastic deformation of an amorphous alloy, J. Appl. Phys. 57 (1985) 3581, https://doi.org/10.1063/1.335013.

[81] A. Zhukov, V. Zhukova, V. Larin, J.M. Blanco, J. Gonzalez, Tailoring of magnetic anisotropy of Fe-rich microwires by stress induced anisotropy, Physica B 384 (2006) 1–4.

[82] Y. Yoshizawa, K. Yamauchi, Fe-based soft magnetic alloy composed of ultrafinegrain structure, Materials transaction JIM 31 (1990) 307–314.

[83] G. Herzer, Anisotropies in soft magnetic nanocrystalline alloys, J. Magn. Magn. Mater. 294 (2005) 99–106.

[84] C. Dudek, A.L. Adenot-Engelvin, F. Bertin, O. Acher, Engineering of the magnetic properties of Finemet based nanocrystalline glass-coated microwires, J. Non-Cryst. Solids 353 (2007) 925–927.

[85] L. González-Legarreta, V.M. Prida, B. Hernando, M. Ipatov, V. Zhukova, A. Zhukov, J. González, Magnetoimpedance dependence on width in $Co_{66.5}Fe_{3.5}Si_{12.0}B_{18.0}$ amorphous alloy ribbons, J. Appl. Phys. 113 (5) (2013) 053905.

[86] M. Ipatov, L. González-Legarreta, J. Garcia, A. Chizhik, L. Domínguez, V. Zhukova, A. Zhukov, B. Hernando, J. González, Induced giant magnetoimpedance effect by current annealing in ultra thin Co-based amorphous ribbons, IEEE Trans. Magn. 49 (2013) 1009.

[87] J.M. Blanco, A. Zhukov, J. Gonzalez, Torsional stress impedance and magneto-impedance in $(Co_{0.95}Fe_{0.05})_{72.5}Si_{12.5}B_{15}$ amorphous wire with helical induced anisotropy, J. Phys. D Appl. Phys. 37 (1999) 3140–3145.

[88] S.D. Jiang, T. Eggers, O. Thiabgoh, D.W. Xing, W.D. Fei, H.X. Shen, J.S. Liu, J.R. Zhang, W.B. Fang, J.F. Sun, H. Srikanth, M.H. Phan, Relating surface roughness and magnetic domain structure to giant magneto-impedance of Co-rich melt-extracted microwires, Sci. Rep. 7 (2017) 46253.

[89] M. Knobel, M.L. Sánchez, C. Gómez-Polo, P. Marín, M. Vázquez, A. Hernando, J. Appl. Phys. 79 (1996) 1646.

[90] A. Zhukov, M. Churyukanova, S. Kaloshkin, V. Semenkova, S. Gudoshnikov, M. Ipatov, A. Talaat, J.M. Blanco, V. Zhukova, Effect of annealing on magnetic properties and magnetostriction coefficient of Fe Ni-based amorphous microwires, J. Alloy. Comp. 651 (2015) 718–723, https://doi.org/10.1016/j.jallcom.2015.08.151.

[91] Jiawen Chen, Jianhua Li, Lixin Xu, Highly integrated MEMS magnetic sensor based on GMI effect of amorphous wire, Micromachines 10 (2019) 237, https://doi.org/10.3390/mi10040237.

[92] P. M-Nowicki, R. Gazda, A. Szewczyk, Marusenkov, A. Nosenko, V. Kyrylchuk, Strain dependence of hysteretic Giant magnetoimpedance effect in Co-Based amorphous ribbon, Materials 12 (2019) 2110, https://doi.org/10.3390/ma12132110.

[93] J. Nabias, A. Asfour, J.-P. Yonnet, Effect of torsion stress on the offset and sensitivity of diagonal and off-diagonal GMI in amorphous wires, Sensors 18 (2018) 4121, https://doi.org/10.3390/s18124121.